

Report to the Texas Coastal Management Program: CMP Cycle 17 Final Report:

If We Lose Follets Island we Lose Coastal Communities and Christmas Bay: A Geological Framework Study and Numerical Model Study of the Sustainability of Follets Island General Land Office (GLO) Contract #13-348-000-7695



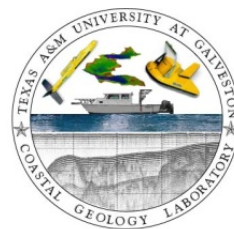
Dr. Timothy M. Dellapenna^{1&2}

Dr. Jens Figlus³

Dr. Joe Carlin,^{1,2&4}

Craig Harter²

Paul Laverty²

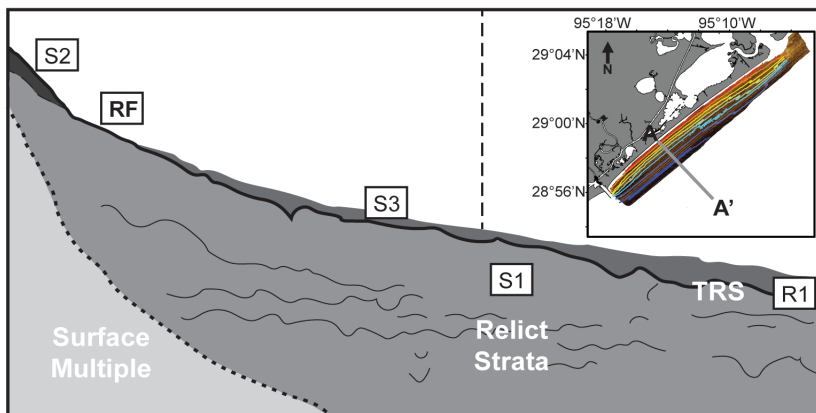


¹Department of Marine Sciences, Texas A&M University at Galveston

²Oceanography Department, Texas A&M University

³Department of Ocean Engineering, Texas A&M University

⁴Department of Geological Sciences, California State University, Fullerton



Department of
Oceanography



TEXAS A&M UNIVERSITY
College of Geosciences

TABLE OF CONTENTS

| | | |
|-----|---|----|
| 1.0 | Introduction | 4 |
| 2.0 | Geophysical Survey and Geological Assessment: Investigating Morphological and Stratigraphic Changes to the Submarine Shoreface of a Transgressive Barrier Island: Follet's Island (FI), Northern Gulf of Mexico | 4 |
| 2.1 | Abstract | 4 |
| 2.2 | Introduction | 4 |
| 2.3 | Study Site | 5 |
| 2.4 | Materials and Methods | 6 |
| | 2.4.1 Survey Design | 6 |
| | 2.4.2 Data Collection and Processing | 6 |
| 2.5 | Results | 8 |
| | 2.5.1 Bathymetric Data | 8 |
| | 2.5.2 Side Scan Sonar Data | 8 |
| | 2.5.3 CHIRP Data | 10 |
| 2.6 | Discussion | 11 |
| | 2.6.1 Transgressive Ravinement | |
| | 2.6.2 Storm-Derived Morphological Changes | 12 |
| | 2.6.3 Understanding Long-term and Short-term Changes to the Shoreface | 13 |
| 2.7 | Conclusions | 15 |
| 2.8 | Acknowledgements | 15 |
| 2.9 | References | 15 |
| 3.0 | Beach and dune monitoring and assessment: <i>The Role of Hurricanes on the Morphological Evolution of a Sediment-Starved Barrier Island along the Upper Texas Coast: Follet's island</i> | 19 |
| 3.1 | Abstract: | 19 |
| 3.2 | Background and Motivation | 19 |
| | 3.2.1 Available Data | 21 |

| | | |
|-----|--|----|
| 3.3 | Data Analysis and Results | 22 |
| | 3.3.1 <i>Metocean</i> | 22 |
| | 3.3.2 <i>Hurricane Ike Hydrodynamics</i> | 23 |
| | 3.3.3 <i>Geomorphology</i> | 23 |
| 3.4 | Discussion and Conclusion | 26 |
| 3.5 | Acknowledgements | 27 |
| 3.6 | References | 28 |
| 4.0 | Modeling: <i>NUMERICAL MODELING OF THE MORPHODYNAMIC RESPONSE OF A LOW-LYING BARRIER ISLAND BEACH AND FOREDUNE SYSTEM INUNDATED DURING HURRICANE IKE USING XBEACH AND CSHORE</i> | 30 |
| 4.1 | Abstract | 30 |
| 4.2 | Background and Motivation | 30 |
| 4.3 | Numerical Models | 33 |
| | 4.3.1 <i>XBeach Background</i> | 33 |
| | 4.3.2 <i>CSHORE Background</i> | 36 |
| | 4.3.3 <i>Model Setup</i> | 37 |
| | 4.3.4 <i>Boundary Conditions</i> | 37 |
| | 4.3.5 <i>Grid Generation</i> | 39 |
| | 4.3.6 <i>Numerical Model Setup</i> | 40 |
| 4.4 | Model Outcomes | 42 |
| | 4.4.1 <i>XBeach Results</i> | 42 |
| | 4.4.2 <i>CSHORE Results</i> | 49 |
| 4.5 | Discussion and Conclusions | 51 |
| 4.6 | Acknowledgements | 52 |
| 4.7 | References | 52 |

| | | | |
|-----|--------------------------|---|----|
| 5.0 | Overall project findings | 56 | |
| | 5.1 | <i>Hurricane Ike impact to the dunes and subaerial island</i> | 56 |
| | 5.2 | <i>Dune and subaerial Island Recovery</i> | 56 |
| | 5.3 | <i>Submarine impact of FI and how this compares to the dune and</i> | 57 |
| 6.0 | Coring supplement | 58 | |

1.0 INTRODUCTION

This is a report of our CMP Cycle 18 project. It was conducted in three phases, which were 1) Geophysical Survey and Geological Assessment, 2) Beach and dune monitoring and assessment, 3) Modeling. Each of these phases has been treated independently and has been written up in publishable manuscripts. Consequently, each phase will be presented here as a separate section with their own methods, results and conclusions sections and an over all conclusion of the entire project is presented at the end of this report, in Chapter 5.

2.0 Geophysical Survey and Geological Assessment:

The field-work associated with this phase was conducted during the summer of 2013. This section was published as a conference paper at the 2015 Coastal Sediments Conference, with the title:

Investigating Morphological and Stratigraphic Changes to the Submarine Shoreface of a Transgressive Barrier Island: Follet's Island (FI), Northern Gulf of Mexico

2.1 ABSTRACT

Barrier islands are increasingly more vulnerable today to the impacts from sea level rise and storms. Therefore, it is important to document the changes from these events, to better understand how these systems may respond in the future. This study investigated the submarine shoreface of FI, located in the northwestern Gulf of Mexico, to document the impact from Hurricane Ike (2008), and longer-term process associated with increases in sea level rise. In 2013, high-resolution swath bathymetry, side scan sonar, and CHIRP subbottom profiling were used to map the island's shoreface. The results showed that the shoreface experienced net erosion from the hurricane. Over the longer-term however, processes associated with sea level rise have resulted in a variety of erosional and depositional areas across the shoreface. These results highlight the complexities of barrier-island-shoreface sedimentation, and give insight to how barrier islands respond to storm events, and rising sea level.

2.2 INTRODUCTION

Barrier Island complexes are frequently found along passive continental margins such as the Atlantic and Gulf Coasts of the United States (Masselink et al., 2005), and dominate the Texas coast. These islands can be classified as one of three types: 1) regressive, 2) aggradational, and 3) transgressive (Galloway and Hobday, 1983). Transgressive barrier islands (TBI) reflect a deficit in the sediment supplied to the island compared to erosion of the shoreface.

Therefore, this type of barrier is particularly vulnerable to accelerated sea level rise, and increased storm frequency resulting from climate change.

Follet's Island (FI), located along the upper Texas coast, is an excellent example of a TBI. FI has a consistent low-elevation profile, with a maximum elevation of ~2 m, making it highly vulnerable to sea level rise, and inundation and high surf from hurricanes and tropical storms. The island has experienced some of the highest shoreline erosion rates along the Texas coast over the past several decades, and was severely impacted by Hurricane Ike in 2008. This storm breached the island in over 75 places and caused dramatic morphological changes to the subaerial portions of the island.

During periods of rising sea level, including extreme events like hurricanes, the barrier island shoreface is where the barrier sequence is modified, truncated or destroyed (Rodriguez et al., 2001). These alterations will directly affect the volume of sand on the beach of the island, and inner shoreface. While changes to the subaerial beach following the event can be dramatic, these changes usually only reflect a small fraction of the total change to the beach and shoreface because they neglect the alterations to the subaqueous portions of the system (Morton et al., 1995). Furthermore, Morton et al. (1995) noted that the subaqueous inner-shelf of barrier islands could be an important sink for beach sands eroded during storm events.

Hurricane Ike made landfall on nearby Galveston Island, with the western eyewall 17 km to the east of the eastern tip of FI, and although FI was on the "clean side" of the hurricane, the island experienced a nearly 3 m storm surge (East et al., 2008), and the storm's impact was dramatic. Between Hurricane Ike (2008) and the mapping of FI (2013) for this study, there were no other tropical storms or hurricanes to impact the study area, so it is assumed that the storm related features observed were the result of Hurricane Ike. The goal of this study, therefore, is to investigate the shoreface of FI to document the response of the system to episodic storms (short time scale), such as Hurricane Ike (Sept. 13, 2008) and as well as rapid sea level rise (longer time scale). Utilizing high-resolution geophysical data including swath bathymetry, side scan sonar (SSS), and CHIRP subbottom profiling collected across the entire shoreface of the island, we investigated features that may have resulted from Hurricane Ike, and those features associated with long-term processes such as increases in sea level. Additionally, bathymetric data was compared to pre-storm data sets to assess the morphological changes following the storm. By combining this morphological data with sedimentological data derived from the SSS and CHIRP, we hope to better distinguish the impacts of sea level rise, and the impacts of the storm on the shoreface of FI, in an effort to better manage the beaches and shoreline in the future.

2.3 Study Site

FI is located along the upper Texas coast (Figure 2.1) in the northwestern Gulf of Mexico (GOM). FI was named after the Follett Family, early settlers in the area, and has been alternatively referred to as Follett's Island and Follets Island, it has also previously been called Velasco Peninsula (Handbook of Texas Online, 2013). The FI is actually a low-elevation peninsula which is generally less than 1 km wide in most areas, less than 25 km long, and bounded by San Luis Pass (SLP) tidal inlet to the east, the Freeport navigational channel (FC) to the west, and Christmas Bay (CB) and the Gulf Coast Intracoastal Water Way (ICWW) on the bay-side of the island. The island itself is a relatively thin (1-4 m) accumulation of transgressive sands overlying fluvial deposits from the nearby Brazos River (Bernard et al., 1970; Morton, 1994; Wallace et al., 2010). On the island's shoreface, the beaches are composed of fine sands, with a series of shore-parallel bars spanning from the toe of the fore-beach, exposed at low tide, out to ~ 3 m water depths (Morton et al., 1994).

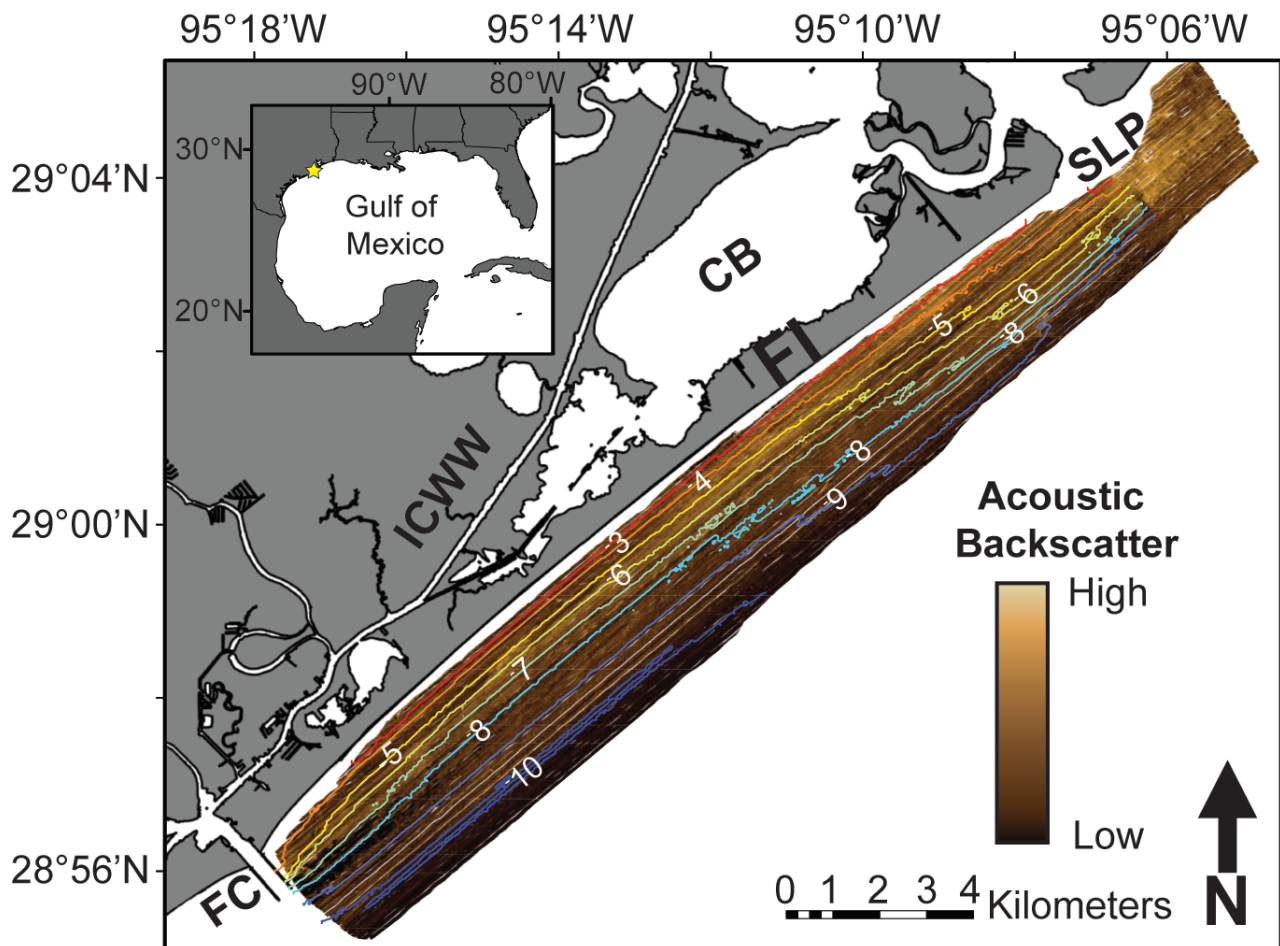


Fig. 2.1. Study area with bathymetric contours overlaid on side scan sonar mosaic. See text for specific location names depicted.

For decades it has been observed that FI is actively eroding (McGowen et al., 1977; Morton and Pieper, 1975; Wilkinson and Basse, 1978). Wallace et al. (2010) described the island as being in a “rollover phase” because the shoreline was eroding at the same rate as the landward movement of the bayline. The principal drivers of shoreline erosion along this coast are deficiencies in sediment supply, increases in relative sea level rise, and storms (Morton, 1979). Storms are an important driver for coastal change on short-term time scales. Increases in wind stress and changes in barometric pressure during seasonal storm events cause changes in water-levels much greater than those resulting from astronomical tides (Morton and Speed, 1998). The typical tidal range for this area is less than 0.5 m, with typical wave heights ~ 1 m, and a net longshore drift that is from the northeast to southwest (Curry, 1960; Nowlin Jr et al., 2005; Seelig and Sorensen, 1973). During storm events, such as hurricanes and tropical storms, wave heights can exceed 7 m at the coast, 22 m in the open Gulf, contribute significantly to the landward transfer of water and beach runup in the form of storm surges, and be responsible for most of the transport of sand in the littoral zone (Morton et al., 1994; Morton and Speed, 1998; Wallace et al., 2010).

2.4 Materials and Methods

2.4.1 Survey Design

The FI survey, conducted in the summer of 2013, spanned the entire 23 km length of the island, and extended 3 km to the east, spanning the width of SLP. In total, the survey area extended from the western tip of Galveston Island, to the Freeport Jetties in the west (Figure 1). All of the surveying was conducted aboard the R/V Cavalla, a 7.6 m Parker® cabins skiff, and covered water depths from less than 3 m to beyond the 10 m isobath based on NOAA nautical charts. Survey lines were plotted parallel to the shore using Hypack® 2013 Coastal Oceanographic software. Line spacing was 100 meters giving 200% coverage for the side scan data, and on average, approximately 60% coverage for the bathymetry data. Bathymetric-data coverage fluctuates with water depths. Survey data was collected in the WGS 1984 datum and projected into UTM Zone 15 North coordinates. The horizontal and vertical data are in meters. The bathymetric data was corrected to mean lowest low water (MLLW) using NOAA tide station 8772447 located at the US Coast Guard station in Freeport, TX located near the western end of the study area.

2.4.2 Data Collection and Processing

Side scan sonar (SSS), and bathymetric data were collected concurrently using a Teledyne Benthos® C3D-LPM High-Resolution Side-Scan Sonar Bathymetric System. This sonar utilizes two transducers operating at a frequency of 200 kHz coupled with a six hydrophone receiver array. The sonar uses a computed Angle of Arrival Transient Imaging (CAATI) algorithm to calculate the water depths across the swath during each sounding. The sonar was pole-mounted to the side of the vessel, positioning was determined using a Hemisphere® Vector

differential GPS and ship motion data were determined using a SG Brown TSS[®] DMS3-05 motion reference unit to correct the bathymetric data collected. Both of these sensors were mounted to the same pole as the sonar to minimize errors, and the need for multiple offset calculations when correcting the sonar data. Periodic casts with an Odom[®] Sound Velocity Probe were conducted to collect sound velocity data throughout the water column to correct bathymetric data. Sonar data were acquired using Hypack[®] Hysweep 2013 software, and the bathymetric data were processed using Hypack[®] Hysweep 2013 software, where tidal, ships motion, and sound velocity data were integrated to correct the raw soundings.

Sub-bottom data were collected using an Edgetech[®] 216 Full Spectrum Sub-bottom CHIRP seismic sonar. This sonar operates on frequencies between 2 and 16 kHz. The vertical resolution of this system is 6 – 10 cm, with typical penetrations ranging from 6 – 80 m depending on bottom type. CHIRP data acquisition was completed using Chesapeake SonarWIZ.Map[®] software. Side scan sonar and CHIRP data were processed using Chesapeake Sonar Wiz.Map[®].

2.5 Results

2.5.1 BATHYMETRIC DATA

The bathymetry data are shown in Figure 1 as the isobaths with a 1 m contour interval. Measured water depths ranged from less than 3 m nearshore, to greater than 10 m in the southwestern corner of the study area. In water depths less than ~ 6 m isobaths trended parallel to the shoreline. In the eastern half of the study area, however, in water depths greater than ~ 6 m we observed a broad, gently sloping platform that extended out ~ 9 m water depths.

2.5.2 SIDE SCAN SONAR DATA

The SSS mosaic is shown in Figure 1, and the mosaic and interpretations are shown in Figure 2. In the mosaic the lighter colors indicate areas of higher backscatter, while darker colors are associated with lower backscatter. It should be noted that SSS gains were normalized in order to enhance contrast over relatively small changes in backscatter intensity. In general, backscatter decreases seaward, although there are two prominent high-backscatter areas observed in the mosaic. One is a large, lobate feature located seaward of the SLP tidal inlet (HBA-1, Figure 2). This feature can likely be attributed to the ebb tidal delta associated with the inlet. The other feature is a band of high backscatter, oriented obliquely to the shoreline, and extending southwestwardly from the eastern section of the island to the jetties at the FC (HBA-2, Figure 2). The mosaic reveals that HBA-2 is more consistent and continuous in the east, but is more discontinuous to the west, separated by bands of low backscatter.

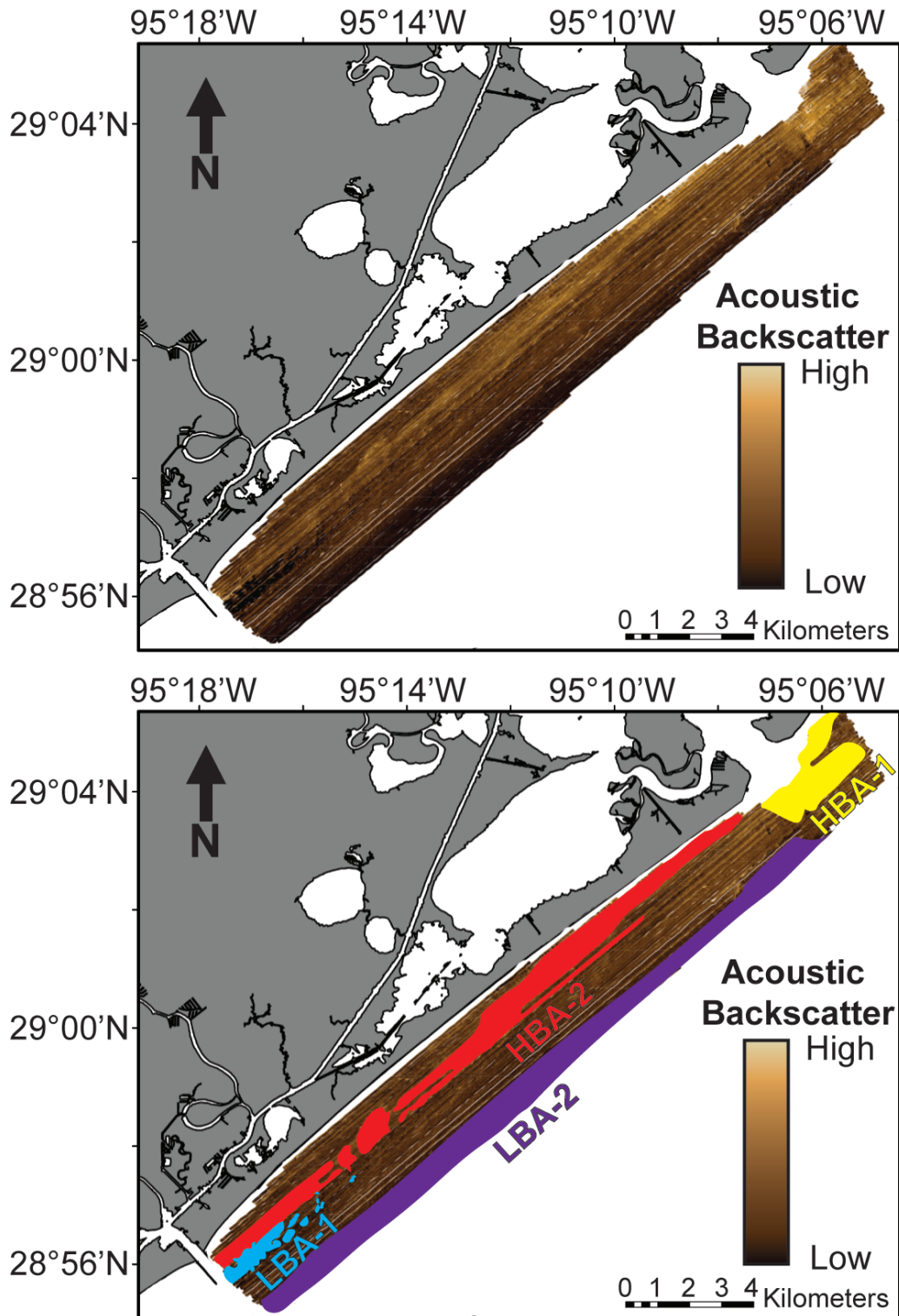


Fig. 2.2. Side scan sonar mosaic (above) with interpretation (below). Features include High Backscatter (HBA-1 yellow, HBA-2 red), and Low Backscatter (LBA-1 blue, LBA-2 purple) Areas.

In addition, a band of distinct, low-backscatter features, that coalesce in some places (LBA-1, Figure 2), were observed in the western portion of the survey area, seaward of HBA-2, and adjacent to the seaward end of the jetties at the FC. From the mosaic, LBA-1 consists of

rounded features that exhibited some of the lowest backscatter intensities observed throughout the study area. From the combined SSS mosaic and isobaths in Figure 1, LBA-1 was located in water depths that ranged from ~ 6 m to ~ 9 m. Overall, much of the low backscatter throughout the survey area was observed in deeper waters (> 8 m water depths), LBA-2 from the mosaic in Figure 2.2.

2.5.3 CHIRP Data

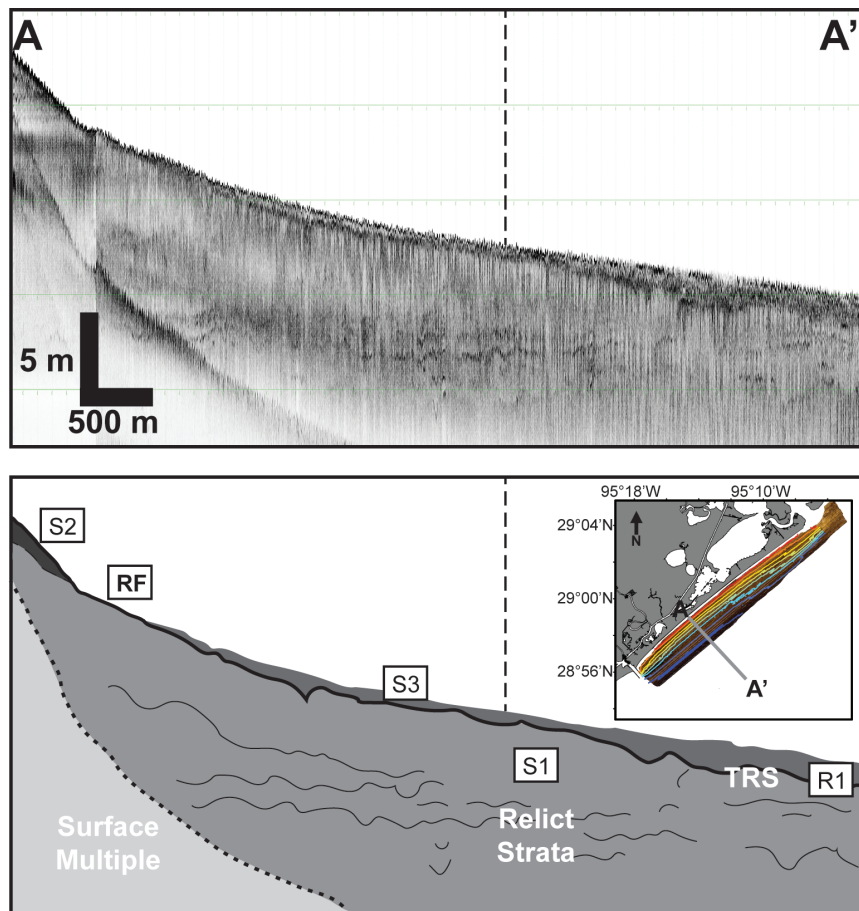


Fig. 2.3. Example of a CHIRP subbottom profile (above) with interpretation (below). See text for explanation of features. Location of profile shown in inset.

Figure 2.3 illustrates a representative shore-normal CHIRP profile from the study area. In general, we observed a thick, subsurface unit with internal reflectors (S1). These internal

reflectors were inconsistent in their orientation (horizontal in areas), and location (more prevalent in the seaward portion of certain transects, other transects in the landward). The surface of this unit is truncated by a prominent reflector (R1) that is consistently overlain by distinct units at the landward (S2) and seaward (S3) extents of the profiles. These units represent the surface units at each end of the profiles respectively, but for sections in the middle of the profiles, R1 represents the seabed, lacking an overlying surface unit. The S2 unit generally thins seaward, and is up to two meters thick. In some areas it contains internal reflectors, these are either parallel to the basal reflector, or seaward dipping. The S3 unit at the seaward end of the profiles is generally thinner, < 1 m in thickness, increasing in thickness in deeper waters. Internally this unit is more acoustically chaotic, lacking any internal reflectors.

2.6 Discussion

2.6.1 *Transgressive Ravinement*

FI is a typical example of a TBI, demonstrating that the island is migrating landward as sea level rises. As a result, the shoreface of the island is undergoing the process of transgressive ravinement, where sediment is progressively reworked landward as fair-weather wave base migrates with sea level rise. This is the defining process for the surface and subsurface morphologies we observed in this study.

In the CHIRP data (Figure 2.3) the R1 reflector represents the transgressive ravinement surface (TRS). The TRS defines the depth of reworking during the ravinement process. Much of the data show that the TRS penetrated into the underlying strata (S1), truncating the surface, and creating an unconformity. The S1 unit therefore, represents relict strata of an undetermined age, likely postglacial (late Pleistocene to early Holocene) during the early stages of sea level rise prior to the formation of the island, or earlier. It is difficult to accurately determine given the current data set, therefore we will refer to it as relict strata, suggesting that it predates deposition related to the island's formation.

Given the ravinement process, the two surface seismic units (S2 and S3) are related to the active process of ravinement. The S2 unit, located at the landward end of the survey is interpreted to be the actively eroding TBI front. This is the toe of the barrier island that is currently eroding as wave base migrates landward during this current transgression. The S3 unit is formed from deposition following the ravinement. This may result from the deposition of marine sediment post-ravinement, or deposition of shoreface sediment that was eroded during the ravinement. With no direct sediment data to determine precisely, we hypothesize that for FI the case may be the latter for reasons we will discuss in detail below.

For this case, we believe that during ravinement, as the S2 unit is eroded, some of that eroded sediment is transported landward as part of the barrier migration, but some is also transported seaward, depositing below wave-base. The latter would contribute to the S3 unit, explaining the deposit overlying the TRS. The ravinement front (RF) exists in the area between these two units, where the TRS intersects the seabed with no overlying surface layer. This is the location on the shoreface where the ravinement processes have completely reworked the entire barrier island sequence down to the underlying relict strata. With ravinement presently occurring at the RF, sediment is prevented from being deposited above the TRS to create the S3 unit. Presumably, as the transgressive ravinement process continues, the RF will migrate landward, and the previous location will become depositional, extending the S3 unit landward.

2.6.2 Storm-Derived Morphological Changes

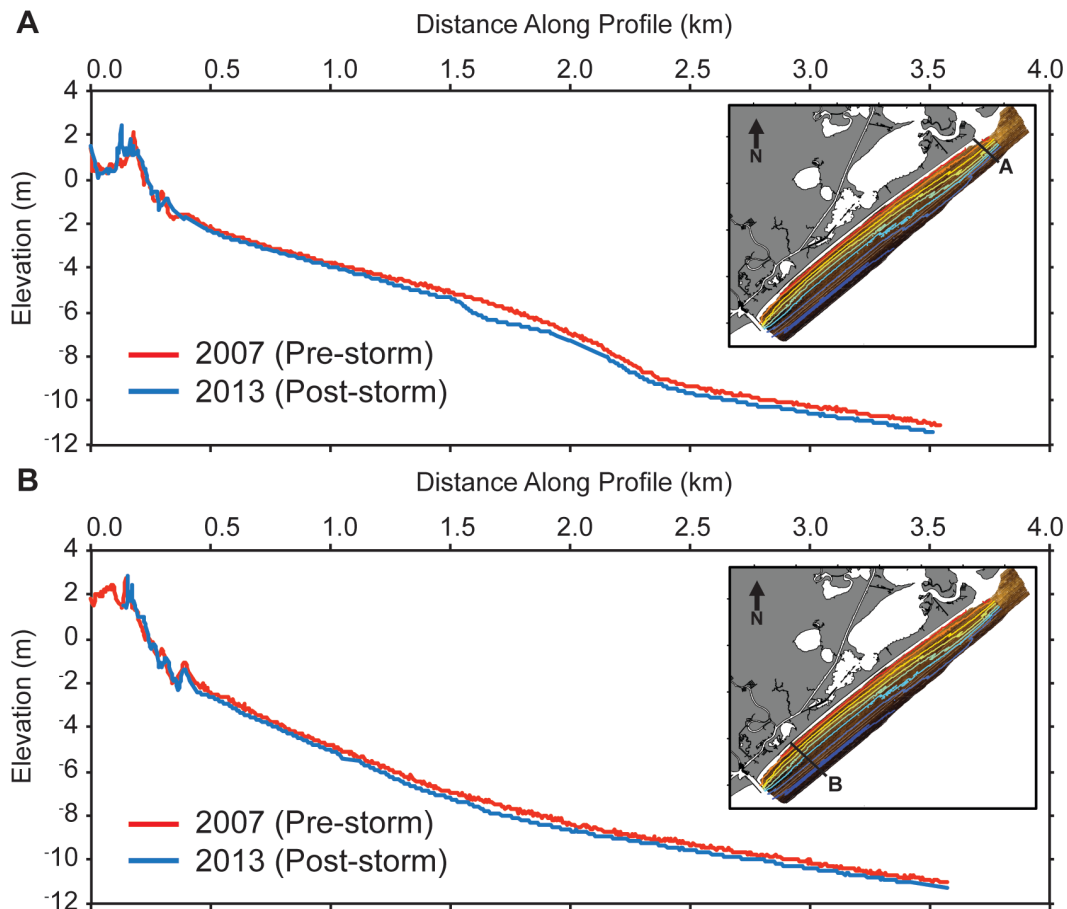


Fig. 2.4. Shoreface bathymetric profiles from before the storm in 2007 (blue) compared to the post-storm profiles from this study (red). Profile locations are shown in panel a.

Utilizing past bathymetric data from before Hurricane Ike, we can investigate the role that this particular storm played in shaping this shoreface, and how these changes compare to what we observed from our CHIRP and SSS data. Beach profile data from 2007 (one year before the storm) was compared to data from the same locations collected in 2013 (five years following the storm), and two representative profiles are shown in Figure 2.4 (for a more detailed discussion on elevation changes on FI resulting from the storm, see Harter et al., this volume).

The overall trend in the data is that the subaqueous shoreface experienced net erosion across the island. Furthermore, because the post-storm data was collected five years following the storm, these data reflect not only the impact from the storm but also the recovery period following the storm. The net change to the shoreface highlights the significant impact this storm had on the island. In some places the shoreface retreated landward up to 180 m, and the volume of sediment lost from the shoreface far outweighed sediment gains on the subaerial beach (Harter et al., this volume).

Additional evidence of storm impacts to the shoreface and the subsequent recovery were also observed in the SSS data. The LBA-1 may be attributed to scour pits that formed during the storm, and subsequently filled with mud either during the storm-surge ebb, or in the years following during the recovery period. Unpublished side scan sonar data collected by Dellapenna in 2001 from this area show no evidence of the scour pits in the area observed in 2013. Similar scour pits were observed on the shoreface of the nearby Matagorda Island as a result of Hurricane Claudette (Majzlik, 2005) in 2003, and also along the adjacent Galveston Island shoreface that can be attributed to Hurricane Ike (Dellapenna and Johnson, 2012). The fact that these features were observed at the far west end of the study area, the furthest distance from the storm's track, indicate that the storm had a significant impact across the entire shoreface of FI.

2.6.3 Understanding Long-term and Short-term Changes to the Shoreface

The changes that resulted from the storm (e.g. scour pits, net shoreface erosion, etc.) represent the short-term changes to the shoreface. While evidence of these event-driven changes may likely be preserved within sedimentary record, it is the longer-term processes associated with typical climatic forcing and sea level rise (e.g. ravinement) that appear to be the dominant driver in shaping the shoreface. These processes create a complex shoreface that consists of both erosional and depositional features.

The erosional features observed along the shoreface include the TBI front, and the RF. The TBI front is currently eroding, but maintains some of the barrier island sequence, whereas, the RF has completely eroded the barrier island sequence down to the relict strata below. These distinctions were observed within the CHIRP and SSS data. For example, HBA-2 corresponds to the RF. The high backscatter associated with this area results because the TRS

intersects the seabed; exposing the consolidated relict strata. The TBI front on the other hand, is slightly lower in backscatter and corresponds to unit S2 in the CHIRP.

Although the shoreface experienced erosion from the storm, over the longer-term there remain areas that are net depositional. The depositional areas include the ebb tidal delta of SLP (HBA-1), and what we are calling the transgressive ravinement deposits. The transgressive ravinement deposits (TRD) are typically low in backscatter on the SSS mosaic, and correspond to LBA-2 on the mosaic, and the S3 unit from the CHIRP. While we cannot say for certain, we believe at least some of the deposits in these areas are derived from the storm surge ebb associated with Hurricane Ike. With the beach and shoreface experiencing a net loss of sediment from the storm, it is likely that some of this sediment was transported landward to the bay-side of the island, and some was also transported seaward of the shoreface. Storm beds seaward of the shoreface are common along the central and south Texas shelf (Rodriguez et al., 2001).

The bathymetry/beach profile data suggests that the storm likely eroded and modified portions of these TRD. The precise nature, and extent to which they were modified is difficult to say given the present data set. Similar deposits observed in CHIRP data from the shoreface of nearby Galveston Island before Hurricane Ike showed a modern mud layer (deposited ~ 40 years prior) with acoustically unique characteristics overlying older (~ 2640 years prior) TRD (Robb et al., 2003). Within the S3 unit on FI there was no evidence of a similar modern mud deposit overlying the TRD, so it is possible that the storm eroded some if not all of a modern mud deposit.

By understanding these morphological and stratigraphic characteristics and distributions we gain a better insight into the processes occurring overtime on the shoreface of the island. Given the nature of the data available and presented here, what we see is that the morphology and stratigraphic record of the FI shoreface is being shaped by the long-term processes, but is punctuated by short-term, episodic events. This interplay between the processes that occur over these various time scales create complexity and heterogeneity across the shoreface. Understanding these complexities, and the impact of these time-variable processes will be important in managing the shoreface, and the shoreline in the future., While the data presented here offers a strong framework for understanding the shoreface processes, a detailed sedimentological/stratigraphic investigation would need to be conducted to better understand the ultimate implications for management. Follow up work is funded and underway from Texas Sea Grant, Texas Coastal Management Program (CMP) and Texas Coastal Impact Assistance Program (CIAP), including a large submersible vibro-coring campaign and instrumented pod deployments (benthic boundary layer dynamics), and modeling efforts, for 2015-2016.

2.7 Conclusions

In conclusion, we see that the shoreface of FI is a dynamic environment, where short-term events such as hurricanes, punctuate the development of the shoreface that evolves through longer-term processes such as changes in sea level rise. The data from this study show that shoreface of FI is complex, consisting of distinct erosional and depositional areas. Additionally, there are areas in which storm-derived features have been preserved (e.g. scour pits, LBA-1). Overall, this study provides a strong framework for understanding the processes occurring on the shoreface of FI over short-time scales (hurricanes), and longer time scales (sea level rise). This study provides a useful framework to better understand the processes driving change on barrier island shorefaces, and has laid the foundation for a more detailed sedimentological/stratigraphic study of the area is underway to provide better data for shoreline and barrier island management.

2.8 Acknowledgements

The authors would like to thank Paul Laverty, Ryan Gay, Judson Crouch, and Kyle Johnson for their help in collecting and processing the data. This project was funded by the Texas General Land Office and NOAA through the Texas Coastal Management Program, Grant number 13-431-000-7890.

2.9 References

- Bartek, L.R., Anderson, J.B., Abdulah, K.C., 1990. The importance of overstepped deltas and interfluvial sedimentation in the transgressive systems tract of high sediment yield depositional systems—Brazos—Colorado deltas, Texas, Sequence Stratigraphy as an Exploration Tool: Concepts and Practices in the Gulf Coast: SEPM, Gulf Coast Section, 11th Annual Research Conference, Program and Abstracts. SEPM, pp. 59-70.
- Belknap, D., Kraft, J., 1981. Preservation potential of transgressive coastal lithosomes on the US Atlantic shelf. *Developments in Sedimentology* 32, 429-442.
- Belknap, D.F., Kraft, J.C., 1985. Influence of antecedent geology on stratigraphic preservation potential and evolution of Delaware's barrier systems. *Marine Geology* 63, 235-262.
- Bernard, H.A., Major Jr, C.F., Parrott, B.S., LeBlanc, R.J., 1970. Recent sediments of southeast Texas—a field guide to the Brazos alluvial and deltaic plains and the Galveston barrier island complex. Austin, TX: University of Texas at Austin, Bureau of Economic Geology.

- Curry, J.R., 1960. Sediments and History of Holocene Transgression, Continental Shelf, Northwest Gulf of Mexico, in: Shepard, F.P., Phleger, F.B., Van Andel, T.H. (Eds.), Recent Sediments, Northwest Gulf of Mexico: A Symposium Summarizing the Results of Work Carried On in Project 51 of the American Petroleum Institute 1951-1958. The American Association of Petroleum Geologists, Tulsa, Oklahoma, U.S.A., pp. 221-266.
- Dellapenna, T. M., Johnson, K., 2012. Mapping and Coring of the Inner shelf of Galveston Island - post Hurricane Ike, Final Report to the Texas Coastal Coordination Council, CMP Cycle 14. Contract No. 10-048-000-3744, Texas A&M University at Galveston.
- East, J.W., Turco, M.J., and Mason, R.R., Jr., 2008. Monitoring inland storm surge and flooding from Hurricane Ike in Texas and Louisiana, September 2008: U.S. Geological Survey Open-File Report 2008-1365 [<http://pubs.usgs.gov/of/2008/1365/>].
- Galloway, W.E., Hobday, D.K., 1983. Terrigenous clastic depositional systems. Applications to petroleum, coal and uranium exploration. New York, NY: Springer.
- "*Handbook of Texas Online* (<http://www.tshaonline.org/handbook/online/articles/rrf01>), Follet's Island. accessed September 29, 2015. Uploaded on June 12, 2010. Modified on February 26, 2013. Published by the Texas State Historical Association.
- Harter, C., Figlus, J., Dellapenna, T., 2015, this volume. Hurricane Impact on the Morphological Evolution of a Sediment-Starved Barrier Island along the Upper Texas Coast. Coastal Sediments (2015). ASCE.
- Kraft J.C., Chrzastowski, M.J., Belknap, D.F., Toscano, M.A., Fletcher III, C.H., 1987. The transgressive barrier-lagoon coast of Delaware: morphostratigraphy, sedimentary sequences, and responses to relative rise in sea level, in Sea-Level Fluctuation and Coastal Evolution, edited by D. Nummedal, O. H. Pilkey, and J.D. Howard, Spec. Publ. Soc. Econ. Paleontol. Mineral. 41, 129-143.
- Majzlik, E.J., 2005. Modification and recovery of the shoreface of Matagorda Peninsula, Texas, following the landfall of Hurricane Claudette: the role of antecedent geology on short-term shoreface morphodynamics. Texas A&M University.
- Masselink, G., Evans, D., Hughes, M.G., Russell, P., 2005. Suspended sediment transport in the swash zone of a dissipative beach. Marine Geology 216, 169-189.
- McGowen, J., Garner, L., Wilkinson, B.H., 1977. The Gulf shoreline of Texas: processes, characteristics, and factors in use. Bur. Econ. Geol. University of Tex. Austin Geol. Curc., 77-3, 27 pp.

- Morton, R.A., 1979. Temporal and spatial variations in shoreline changes and their implications, examples from the Texas Gulf Coast. *Journal of Sedimentary Research* 49.
- Morton, R.A., 1994. Texas barriers, *Geology of Holocene Barrier Island Systems*. Springer, pp. 75-114.
- Morton, R.A., Gibeaut, J.C., Paine, J.G., 1995. Meso-scale transfer of sand during and after storms: implications for prediction of shoreline movement. *Marine Geology* 126, 161-179.
- Morton, R.A., Paine, J.G., Gibeaut, J.C., 1994. Stages and durations of post-storm beach recovery, southeastern Texas coast, USA. *Journal of Coastal Research*, 884-908.
- Morton, R.A., Pieper, M.J., 1975. Shoreline changes in the vicinity of the Brazos River delta (San Luis pass to Brown Cedar Cut). An analysis of historical changes of the Texas Gulf shoreline. *Bur. Econ. Geol. University of Tex. Austin Geol. Curc.*, 75-4.
- Morton, R.A., Speed, F.M., 1998. Evaluation of shorelines and legal boundaries controlled by water levels on sandy beaches. *Journal of Coastal Research*, 1373-1384.
- Nowlin Jr, W.D., Jochens, A.E., DiMarco, S.F., Reid, R.O., Howard, M.K., 2005. Low-Frequency Circulation Over the Texas-Louisiana Continental Shelf, in: Sturges, W., Lugo-Fernández, A. (Eds.), *Circulation in the Gulf of Mexico: observations and models: Geophysical monograph series*. American Geophysical Union, Washington D.C., pp. 219-240.
- Robb, B.K., Allison, M.A., and Dellapenna, T.M., 2003. Anthropogenic and natural controls on shoreface evolution along Galveston Island, Texas. *Proceedings of the International Conference on Coastal Sediments 2003. CD-ROM Published by World Scientific Publishing Corp. and East Meets West Productions, Corpus Christi, Texas, USA*. ISBN 981-238-422-7, 13p.
- Rodriguez, A.B., Fassell, M.L., Anderson, J.B., 2001. Variations in shoreface progradation and ravinement along the Texas coast, Gulf of Mexico. *Sedimentology* 48, 837-853.
- Seelig, W.N., Sorensen, R.M., 1973. Investigation of Shoreline Changes at Sargent Beach, Texas, TAMU-SG-73-212 ed. Texas A&M University Sea Grant, p. 153.
- Wallace, D.J., Anderson, J.B., Fernández, R.A., 2010. Transgressive ravinement versus depth of closure: A geological perspective from the upper Texas coast. *Journal of Coastal Research* 26, 1057-1067.
- Wilkinson, B.H., Basse, R.A., 1978. Late Holocene history of the central Texas coast from Galveston Island to Pass Cavallo. *Geological Society of America Bulletin* 89, 1592-1600.

Wright, L.D., Coleman, J.M., 1972. River delta morphology: wave climate and the role of the subaqueous profile. *Science* 176, 282-284.

3 Beach and dune monitoring and assessment

This section was published as a conference paper at the 2015 Coastal Sediments Conference, with the title:

The Role of Hurricanes on the Morphological Evolution of a Sediment-Starved Barrier Island along the Upper Texas Coast: Follet's island

3.1 Abstract:

LiDAR and bathymetric surveys were used in conjunction with aerial imagery to evaluate the impact of Hurricane Ike (2008) on Follet's Island (FI), a sediment-starved barrier island on the Upper Texas Coast. Elevations from LiDAR surveys were interpolated onto cross-shore transects, documenting the coastal response of the beach and dune system to the passing of Ike, as well as five years of subsequent recovery. Pre-Ike and post-Ike bathymetric surveys were compared along these transects to evaluate the long-term impact of Ike to the subaqueous shoreface. It was found that the beach and dune systems experienced a net increase in sediment volume and an advancement of the shoreline after five years of recovery. This increase to the subaerial portion of the island represents less than 5% of the subaqueous volume loss to the shoreface. Sediment carried to the nearshore and back barrier by Hurricane Ike replenished sediment to FI that had been lost to decades of starvation, allowing nearshore and aeolian processes to then restructure the island. This raises the question of whether hurricane overwash is critical to sustaining barrier islands in starved systems, and if so, whether coastal management strategies should be reconsidered for sediment starved barrier islands.

3.2 Background and Motivation

In many places along the U.S. East and Gulf Coast, barrier islands are the first line of defense against extreme weather events threatening our coastlines. The morphological evolution of barrier islands depends on both long-term and short-term processes and is inherently linked to local sediment availability (Zhang, 2004). Unfortunately, only limited data are available to quantify or predict the morphological evolution of barrier islands. The goal of this study is to better understand the dynamics of morphological changes in barrier island systems caused by extreme events since their compounding effects play a critical role in the long-term evolutionary trends of our coastlines. As an example, Follet's Island (FI), a sediment-starved barrier island along the Upper Texas Coast (UTC) is used here. The UTC is characterized by long, narrow barrier islands comprised of fine sand (less than 0.2 mm), and a microtidal wave dominated hydrodynamic environment (Morton et al., 1994; Mason et al., 1981). FI is one of the most vulnerable stretches of the UTC due to its narrow width and high background erosion rates. The island is 25 km long, low-lying (-0.14 m – 2.06 m NAVD88), ranges between

only 0.23 - 0.45 km in width and contains a series of beach communities, including Treasure Island and Surfside. In addition, FI protects important economic and ecological assets like Christmas Bay, the Brazoria National Wildlife Refuge, the Blue Water Highway, the Gulf Intracoastal Waterway (GIW), and parts of the port of Freeport including the Naval Petroleum Reserve and an LNG de-liquification plant (Figure 3.1).

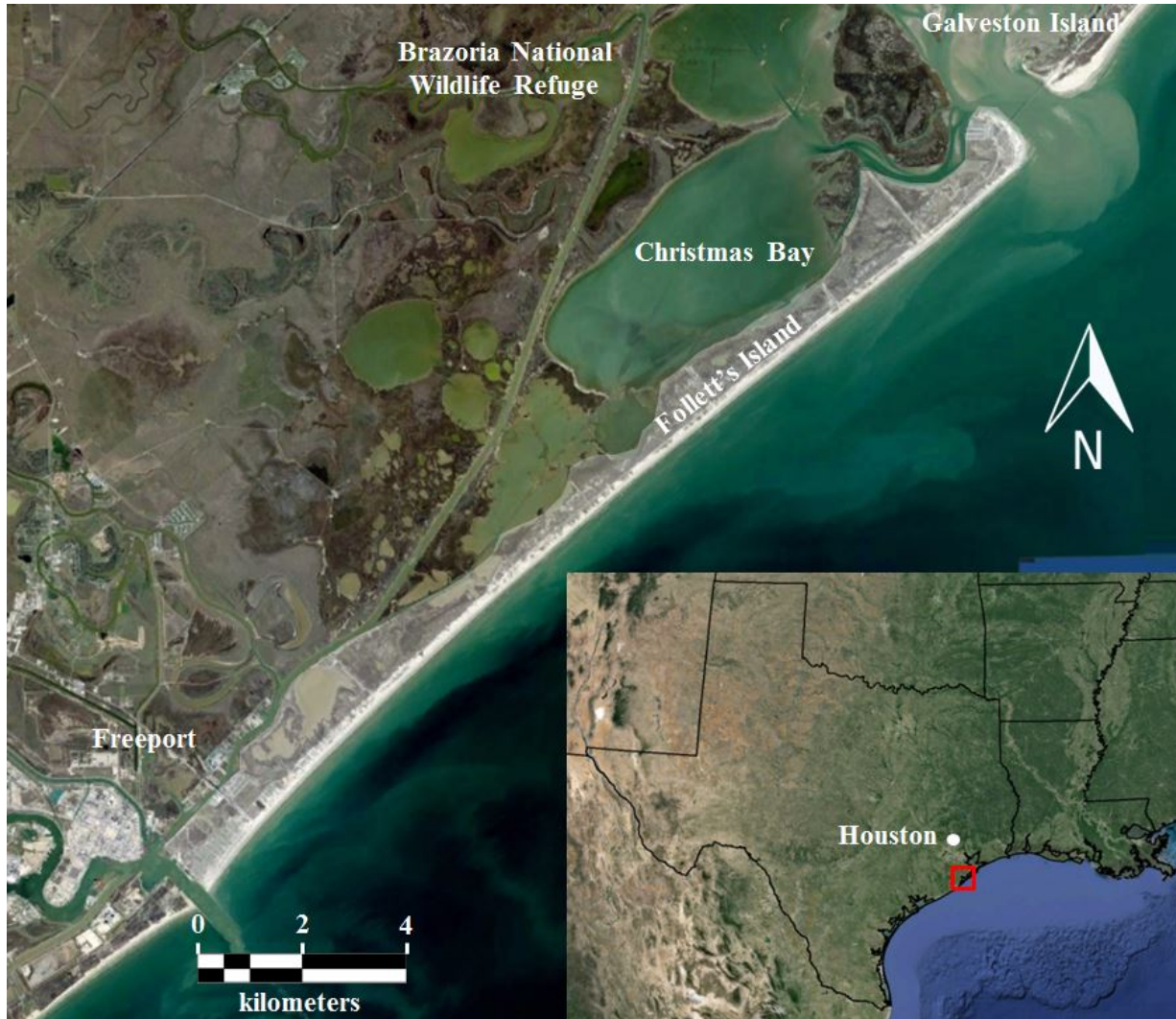
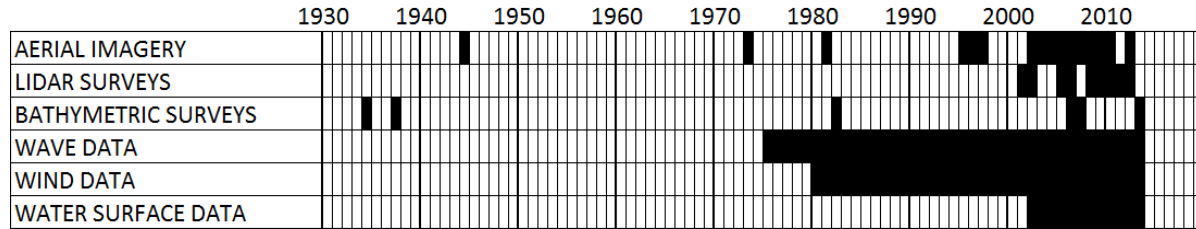


Fig. 3.1. Map of FI showing its position along the Upper Texas Coast

The Brazos River, a major sediment source for FI, was rerouted 6.5 miles west of the Freeport jetties in 1929. This, in conjunction with damming upriver resulted in a sediment deficit on FI (Morton and Pieper, 1975; Mason, 1981). Thus, FI experiences alarming rates of long-term erosion, with shoreline retreat ranging from -1.5 m/yr and -3.9 m/yr (Paine et al., 2011). In 2008, FI was breached in over 75 places by Hurricane Ike, resulting in major damage and severe changes to the island morphology. In this study we observe the morphological evolution of FI based on hydrodynamic forcing conditions during Ike using pre- and post-storm LIDAR surveys and aerial imagery in conjunction with topographic and bathymetric profile surveys. These data will ultimately be used in further research as a baseline for



numerical model simulations of barrier island morphodynamics (CSHORE and XBeach) to calibrate the models for such scenarios.

Fig. 3.2. Overview of available historical data for Follet’s Island. Black fields indicate availability.

3.2.1 Available Data

One of the greatest challenges of studying FI, is the modicum of available historical data; particularly bathymetric data. A comprehensive set of available physical data relevant to the morphological history of FI was compiled in this study. These data arise from scouring online data archives from organizations like the National Oceanographic and Atmospheric Administration (NOAA), The United States Geological Survey (USGS), and the Texas Natural Resources Information System (TNRIS) as well as from direct correspondence with the Texas General Land Office (GLO). An overview of available data is shown in Figure 3.2.

Although aerial imagery of FI is available as far back as 1944, the bulk of this imagery is available after 1995. These images have resolutions between 35 cm and 1 m. LiDAR surveys are available almost annually after 2001. These surveys are provided either as a 1 m resolution DEM raster or as a scatter point cloud with point density between 0.27 – 0.39 pts/m². The LiDAR surveys after 2006 record the topographic response of the FI dune and beach system to Hurricane Ike as well as the subsequent recovery. Bathymetric surveys range in coverage area and resolution, but two surveys from 2007 and 2013 offer profile elevations along similar cross-shore transects. Since there are no National Data Buoy Center (NDBC) Stations proximate to FI with directional wave data historical records, hindcast wind and wave data from the Wave Information Studies (WIS) Station 73066 located offshore of FI in 16 m water depth were analyzed to obtain a better understanding of the general forcing conditions at the project location. Validation with the nearest NDBC station shows that WIS hindcast data is accurate for representing the mean wave direction although some studies have shown the WIS data tend to underestimate significant wave height in winter months due to errors in modeling mature swell (Tracy, 1999; Hanson et al., 2009). A temporary monitoring network of pressure transducers was deployed by the USGS at 65 locations on the gulf coast (East et al, 2008). One of these instruments, SSS-TX-GAL-015 was positioned at the San Luis Pass and provided a time series of surge elevation and barometric pressure near FI. Kennedy et al. (2011) deployed temporary wave gauges in nine locations offshore of the Texas coastline in 8-

16 m water depth to record wave data during Ike. Gauges W and V, positioned at the eastern and western ends of FI respectively, provide time series of significant wave height, peak period and mean water level offshore of FI during the storm.

3.3 Data Analysis and Results

3.3.1 *Metoccean*

Wind and wave roses comprising wave heights, wind speeds and wind/wave directions from 1980 to 2013 are shown in Figure 3.3. From these it is clear that the prevailing wind and wave direction is from SSE and SE, resulting in a dominant westward flow of sediment (Mason et al., 1981; Wallace et al., 2010). Although the winds from SSW and SW occur more regularly, a proportionally greater percentage of peak winds (>10 m/s) are from the north, representing frequent cold fronts passing through the area during winter months (Nov – Apr).

On the average, there are 46 cold fronts per year that pass through the northern Gulf of Mexico (Henry 1979). Cold fronts occur at 3-10 day intervals in a given year and are characterized by a pre-frontal phase of high-energy southeasterly winds for 1 to 2 days, followed by a 12 to 24 hour

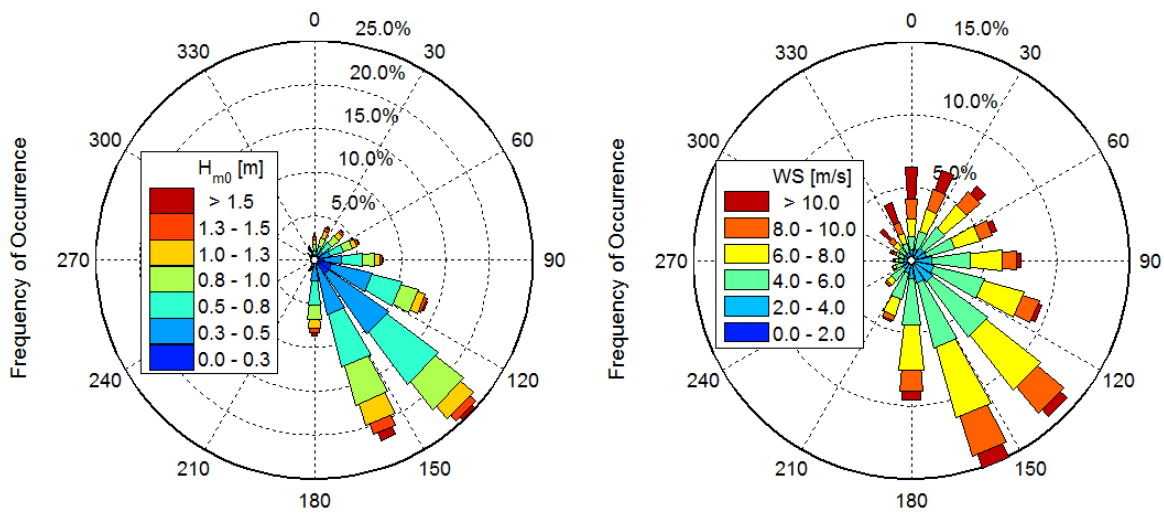


Fig. 3.3. (Left) Wave Rose and (Right) Wind Rose comprising wind and wave data from 1980 to 2013 at WIS Station 73066.

period of strong northwesterly to northeasterly winds following the passage of the front (Cops 2005). Along Galveston Bay, including Christmas Bay, water levels in the bay can be lowered by as much as 1.5 m during the passage of a severe cold front and typically are lowered by at least 0.5 m. These cold fronts play a critical role in the recovery of barrier

islands after a storm by creating an elevated backbeach that ultimately nourishes the existing dune or forms a new dune system (Morton et al., 1994). Cold fronts also cause erosion of the bayside beach from locally generated northerly waves (Stone et al., 2004).

3.3.2 Hurricane Ike Hydrodynamics

Storm surge at FI reached a peak storm elevation of 2.6 m NAVD88. This peak was preceded by a forerunner surge of about 1 m beginning approximately 18 hours before landfall, after which the water level steadily rose to 2.2 m NAVD88 over the next 12 hours. This flooded Christmas Bay and the back barrier region well before Ike made landfall. Waves offshore of FI exceeded 4.5 m significant wave height at 16 second peak period. After landfall, the water level quickly dropped to 2 m NAVD88 over the course of 12 hours. The amount of inland flooding from the forerunner resulted in a strong ebb flow that scoured large channels in FI as the water dragged sediment back out to the gulf.

3.3.3 Geomorphology

Land elevations derived from LiDAR surveys in 2006 and 2010 – 2012 were interpolated onto 8 cross-shore transects (Figure 3.4). These transects are spaced between 2 and 5 km along the length of FI and are aligned with single beam bathymetric profiles from surveys conducted in 2007 and 2013. The 2013 survey also includes topographic data covering the area between the road and the shoreline.

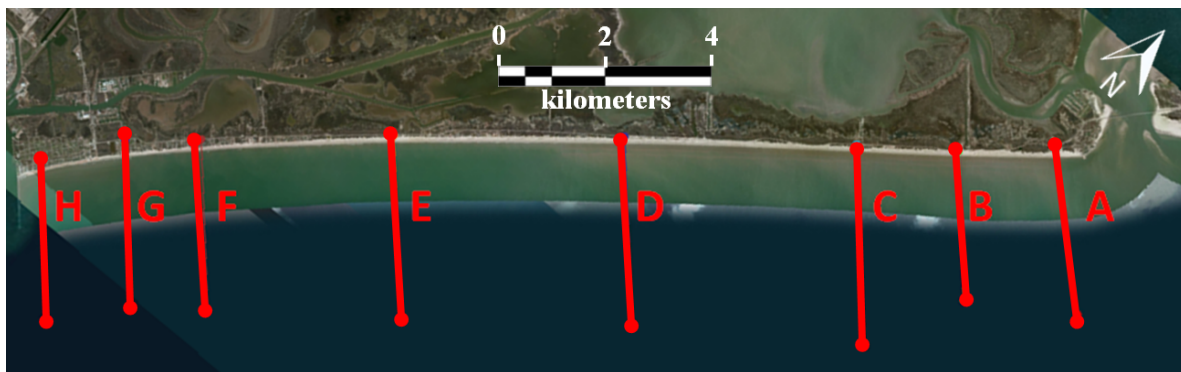


Fig. 3.4. Cross-shore transects for analysis of island topography and bathymetry

After Ike, the more densely populated west side of FI underwent a series of construction projects including a revetment construction and beach nourishment project. Thus, Sections F - H were excluded from this analysis as they do not reflect the islands natural recovery. The elevations from the combined 2006 LiDAR survey and 2007 bathymetric survey are assumed to represent the pre-Ike conditions. There was one smaller hurricane (Hurricane Humberto) that made landfall about 100 km east of FI in 2007 (Blake, 2007), but the short life of this hurricane resulted in minimal impacts to the coast.

Morton (1994) observed the recovery of nearby Galveston Island in the wake of Hurricane Alicia. It was found that recovery occurred in four stages: (1) rapid forebeach accretion, (2) backbeach aggradation, (3) dune formation and (4) dune expansion and vegetation recolonization. It was found that the maximum recovery was reached after an average of four years, after which time the barrier island resumed its regular long-term trend.

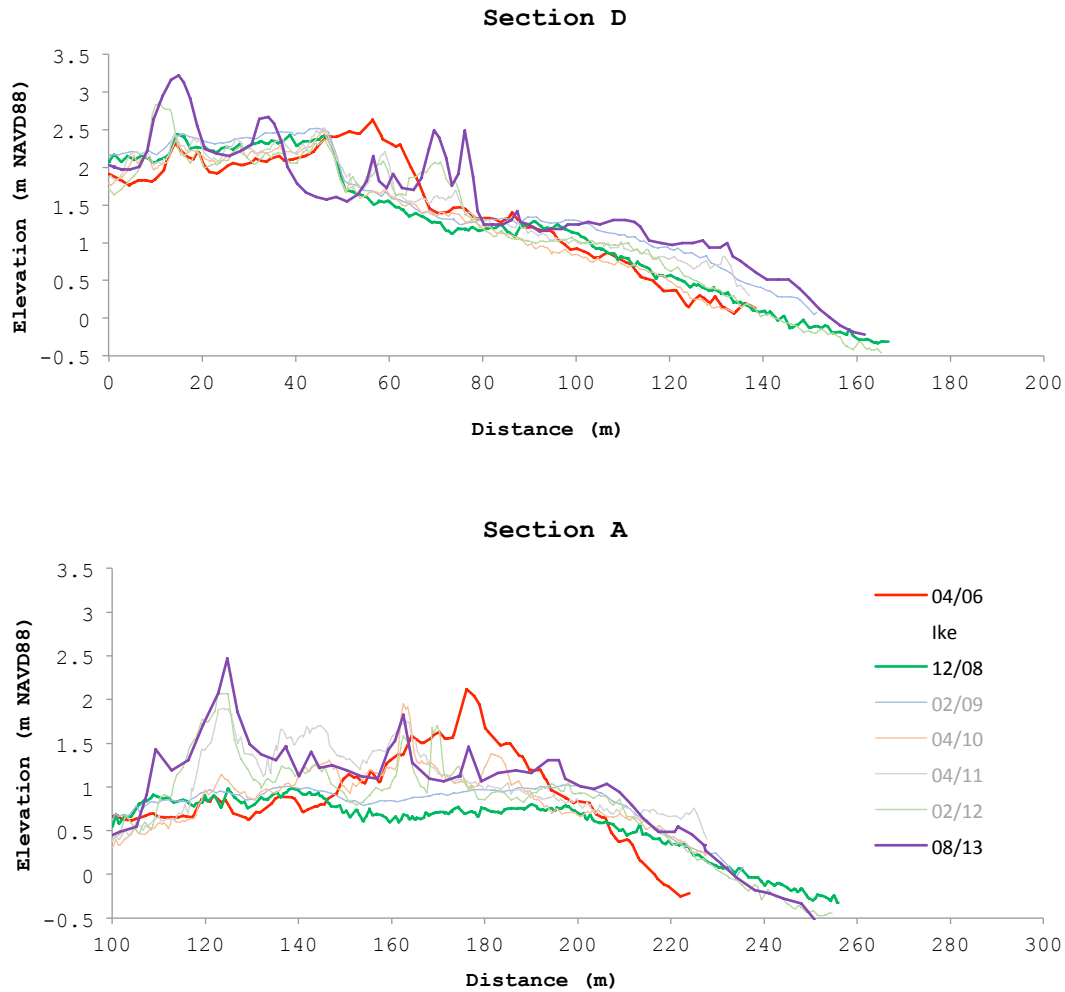


Fig. 3.5. Elevation profiles documenting the impact of Hurricane Ike to the dune and beach as well as the subsequent recovery period at Sections A & D

Figure 3.5 shows the profiles of the dune and beach for Sections A and D from the pre-storm conditions (2006) and for approximately five years of recovery after Ike. These sections most clearly represent the post-storm morphology trends of the east end of the island (Sections A-C) and the center of the island (Sections D-E) respectively. It is clear from these surveys that the original dune was demolished by Ike, depositing sediment both in the back barrier during overwash and on the forebeach/offshore during return flow. This deposition on the

forebeach acted to flatten the beach slope and extend the shoreline slightly seaward. Initial beach slopes range from 25H:1V to 50H:1V, while post-Ike beach slope was universally around 55H:1V.

The first five months of recovery of the FI dune and beach system are characterized by rapid accretion of the forebeach followed by backbeach aggradation (where a backbeach exists). By April 2010, the new dune system had begun to form, and between 2010 and August 2013, the dunes increased in volume while the beach steepened slightly. This recovery process parallels that observed by Morton (1994) and can mainly be attributed to accumulation of aeolian sediment transport.

Table 3.1

| | Section E | Section D | Section C | Section B | Section A |
|-------------|------------------|------------------|------------------|------------------|------------------|
| 2008 | 2.0% | 3.0% | -21.0% | -33.3% | -5.0% |
| 2009 | 10.2% | 11.0% | -19.5% | -19.3% | 1.6% |
| 2010 | -2.8% | -5.8% | -23.9% | -28.4% | 1.6% |
| 2011 | 5.9% | 3.7% | -15.3% | -18.6% | 14.9% |
| 2012 | 7.4% | 9.6% | -16.3% | -18.6% | 13.1% |
| 2013 | 22.9% | 18.2% | -2.1% | 4.3% | 25.7% |

Sediment volume change (erosion -, accretion +) to the dune and forebeach as a percentage of the pre-Ike sediment volume.

Toward the eastern end of the island, the new dune developed landward of the original dune, while in the center of the island the new dune developed at the same location or seaward of the original dune. All profiles showed an advancing of the shoreline from the original shoreline position. For each profile, the volume of sand between the back of the dune and the shoreline above Mean Low Tide (MLT) was calculated. These values are shown in Table 3.1 as a percentage of the pre-Ike volume for each survey date. With the exception of Section C, all sections showed a net gain in sediment volume (up to 25%) after five years of recovery. Each section had a volume recovery of 20-30% from the post-Ike profile. However, on the east end of the island, Sections B & C experienced an initial volume loss of 20-30% so that they only recovered to approximately the same volume as the pre-Ike profile. Alternatively, in the middle of the island, the sediment volume remained roughly the same immediately after Ike and subsequently increased over the recovery period. The large initial volume loss at Sections B & C is likely caused by the storm surge ebb being more severe at these sections due to their lower elevation.

There were no bathymetric surveys conducted near FI immediately after the passing of Ike, so it is difficult to determine how the nearshore bathymetry changed during the storm. The topographic/bathymetric survey conducted in 2013 was used to evaluate the shoreface elevation after five years of recovery. Figure 3.6 shows the offshore profiles from pre-storm and post-recovery scenarios on representative Section A. It is clear from this figure that the shoreface (subaqueous) has retreated by up to 180 m despite the advancing shoreline (subaerial). This loss in sediment continues offshore to well below a conservative estimate of the depth of closure of -8 m (Wallace et al., 2010), and thus it is likely that the bulk of this loss occurred during the hurricane, depositing sediment along the inner shelf, seaward of our profile data and within the back barrier regions, including the fringing marshes and the open bay. It should be noted that the net volume gain to the subaerial beach and dune represent less than 5% of the net sediment loss to the subaqueous shoreface.

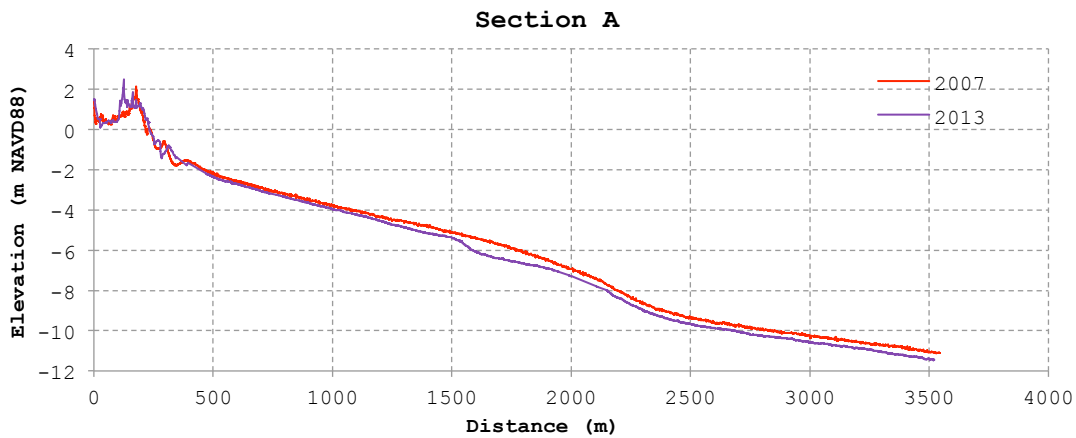


Fig. 3.6. Offshore profiles for pre-Ike and post-recovery conditions at Section A

3.4 Discussion and Conclusion

Hurricane Ike was one of the most destructive storms to ever hit the UTC. Interestingly, this storm resulted in a net gain of sediment volume in the dune and subaerial beach after five years of recovery, where large storms typically result in a net loss. In fact, there was a net loss of sand to the FI system, and although the dunes grew, this dune growth represents retention of only approximately 5% of the total sand lost from the subaqueous shoreface. However, there was a 25-30% growth in volume of the subaerial portion of the island. This appears to be a bit of a paradox; however it can be explained conceptually. FI was overwashed by Ike with a 1 m storm surge that lasted over 30 hours and a 2.2 m storm surge that lasted over 12 hours. During nearly all of the period of time during the storm surge, there were onshore directed winds and waves. This was followed by a rapid offshore directed storm surge ebb,

the initial phase of which would have been both across the island as well as through the 75 storm surge ebb channels cut through the island. The LIDAR data presented here is only for the portion of the island seaward of Hwy 257, which extends along the length of FI. The 12/2008 LIDAR survey shows that the dunes were largely destroyed by Ike and that most of the subaerial portion within this coverage was flattened. With the passage of an average of 46 cold fronts a year, between Ike and the 2013 LIDAR, there were between 200-250 cold fronts that passed through the area, of varying intensities. The LiDAR data show washover deposits landward of the original dune immediately after Ike. These deposits would receive the brunt of the northern winds when the fronts pass, resulting in significant bay towards beach aeolian transport of sand.

Barrier islands along the northern Gulf of Mexico are oriented generally in a east-west to northeast-southwest orientation. As a result, the back bay areas are significantly impacted by northern fronts. Bay to barrier island transport, as part of the recovery of barrier islands from hurricane overwash is seldom, if ever considered. This study demonstrates that with barrier island overwash, that during the recovery phase, bay to beach transport of sand can not only build the dunes back to pre-hurricane conditions, they can actually build dunes up to be larger than pre-hurricane conditions in spite of significant erosion of the shoreface. These observations have significant implications for barrier island management. Perhaps, rather than creating an elevated structures, such as seawalls and dikes to prevent overtopping, the dune system should be left in its natural state. Additionally, perhaps rather than awaiting a hurricane to replenish a barrier island's sediment supply, nourishment projects could be considered for the back barrier or for nearshore berms. For continued research, it will be interesting to examine smaller storms, for which no dune overtopping occurs, and whether this case results in a net loss of sediment volume and a retreating shoreline.

3.5 Acknowledgements

This publication was supported by grants from the Texas General Land Office and NOAA through the Texas Coastal Management Program, Grant number 13-431-000-7890 and from an Institutional Grant (NA14OAR4170102) to the Texas Sea Grant College Program from the National Sea Grant Office, National Oceanic and Atmospheric Administration, U.S. Department of Commerce. In addition, support during the data mining process was also provided by the Texas General Land Office and Coast & Harbor Engineering, a Division of Hatch-Mott McDonald.

3.6 References

- Blake, E.S. (2007). "Tropical Cyclone Report: Hurricane Humberto (AL092007)," *Tech Rep.* National Hurricane Center, Miami, FL.
- Co-ops (2005). On-line Data-base, WWW page, <http://co-ops.nos.noaa.gov/index.html> station, Station 8771341 Galveston Bay Entrance, North Jetty, Texas. *Center for Operational Oceanographic Products and Services, U. S. National Oceanographic and Atmospheric Administration*
- East, J. W., Turco, M. J., & Mason, R. R. (2008). *Monitoring inland storm surge and flooding from Hurricane Ike in Texas and Louisiana, September 2008.* U. S. Geological Survey.
- Hanson, J. L., Tracy, B. A., Tolman, H. L., & Scott, R. D. (2009). "Pacific hindcast performance of three numerical wave models," *Journal of Atmospheric and Oceanic Technology*, 26(8), 1614-1633.
- Henry, W. K. (1979). "Some aspects of the fate of cold fronts in the Gulf of Mexico," *Monthly Weather Review*, 107(8), 1078-1082.
- Kennedy, A. B., Gravois, U., & Zachry, B. (2010). "Observations of landfalling wave spectra during Hurricane Ike," *Journal of Waterway, Port, Coastal, and Ocean Engineering*, 137(3), 142-145.
- Mason, C. (1981). "Hydraulics and stability of five Texas inlets," *Tech Rep. No. CERC-MR-81-1*, Coastal Engineering Research Center, Fort Belvoir, VA.
- Morton, R.A., Pieper, M.J., 1975. "Shoreline changes in the vicinity of the Brazos River delta," *University of Texas, Bur Econ Geol, Geol Circ*, 75-4.
- Morton, R. A., Paine, J. G., & Gibeaut, J. C. (1994). "Stages and durations of post-storm beach recovery, southeastern Texas coast, USA," *Journal of Coastal Research*, 884-908.
- Paine, J.G., Mathew, S., and Caudle, T. (2011). "Texas Gulf Shoreline Change rates through 2007," *Tech Rep. contract no. 10-041-000-3737*. Bureau of Economic Geology, The University of Texas at Austin, Austin, TX.
- Stone, G. W., Liu, B., Pepper, D. A., & Wang, P. (2004). "The importance of extratropical and tropical cyclones on the short-term evolution of barrier islands along the northern Gulf of Mexico, USA," *Marine Geology*, 210(1), 63-78.
- Tracy, B. A. (1999). "Directional Characteristics of the 1990-1999 Wave Information Studies. Gulf of Mexico Hindcast," *Engineer Research and Development Center, Coastal and*

Hydraulics Lab, Vicksburg,

Wallace, D.J., Anderson, J.B., Fernández, R.A. (2010). "Transgressive ravinement versus depth of closure: A geological perspective from the upper Texas coast," *Journal of Coastal Research* 26, 1057-1067.

Zhang, K., Douglas, B., & Leatherman, S. (2002). "Do Storms Cause Long-Term Beach Erosion along the US East Barrier Coast?" *The journal of Geology*, 110(4), 493-502.

4.0 Modeling

This section has been formatted for publication but has yet to be submitted, it is still in revision and is provided here in its current state. It should be noted that a Texas Sea Grant Project was also funded, where this CMP project was used as a basis for the data for the Sea Grant project and was used to leverage additional support. The modeling portion of this study will continue as part of the Texas Sea Grant project. The working title of this manuscript is:

Numerical Modeling of the Morphodynamic Response of a Low-lying Barrier Island Beach and Foredune System Inundated during Hurricane Ike using XBeach and CSHORE

4.1 Abstract

Follet's island (FI) is a sediment-starved barrier island located on the Upper Texas Coast; a stretch of coastline along the Gulf of Mexico that experiences on average four hurricanes and four tropical cyclones per decade. During Hurricane Ike, water levels and wave heights at FI exceeded the 100-year and 40-year return values, respectively, leading to significant overtopping and morphology changes of this low-lying barrier island. The physical processes governing the real-time morphodynamic response of the beach and dune system during 96 hours of hurricane impact were modeled using XBeach (2D) and CSHORE (1D). Hydrodynamic boundary conditions were obtained from ADCIRC/SWAN model runs validated with measured buoy and wave gauge data while LiDAR surveys provided pre- and post-storm measured topography.

XBeach displayed a decent model skill of 0.34 and was very useful in qualitatively visualizing erosion and deposition patterns. CSHORE also displayed a decent model skill of 0.33 and was able to accurately predict the post-storm beach slope and shoreline, but was less effective at simulating the foredune morphology. Modeling results show that the complete morphodynamic response of FI to Hurricane Ike was governed by a sequence of four distinct interaction regimes, including impact, overwash, inundation, and storm surge ebb.

4.2 Background and Motivation

In many places along the U.S. East and Gulf Coast, barrier islands are the first line of defense against extreme weather events threatening our coastlines. The morphological evolution of barrier islands depends on both long-term and short-term processes and is inherently linked to local sediment availability (Zhang, 2004; Leatherman et al., 1983). Unfortunately, only limited data are available to quantify or predict the morphological evolution of barrier islands. The goal of this study is to better understand the dynamics of morphological changes in barrier island

systems caused by extreme events, since their compounding effects play a critical role in the long-term evolutionary trends of our coastlines and a better understanding of the governing processes will lead to improved coastal management strategies. As a case study, Follet's Island (FI), a sediment-starved barrier island along the Upper Texas Coast (UTC) is examined.

The forcing conditions driving the morphodynamics of barrier islands during storms are characterized by four impact regimes as outlined by Sallenger (2000): swash, collision, overwash and inundation. During the swash regime, swash motions reach only as high as the dune toe, and sediment is pulled from the beach offshore. The collision regime is characterized by waves directly impacting and eroding the dune face. During the overwash regime, wave runup levels exceed the dune crest, allowing washover sediments to be deposited on the back side of the dune. Finally, during the inundation regime, the storm surge level exceeds the dune crest, causing high velocity overwash flows and wave penetration to the back-bay.

FI experienced all of these regimes during the passage of Hurricane Ike in 2008, including a prolonged collision regime due to a forerunner surge that preceded the storm surge. Additionally, FI experienced significant morphological changes due to the ebbing storm surge after the hurricane made landfall. This additional morphodynamic forcing condition caused by gravity-driven flow from the bay to the ocean has been investigated by several researchers (e.g. Hayes, 1967; Thieler and Bush, 1991; Lennon, 1991, Tedesco et al., 1995; Goff et al., 2010; and Sherwood et al., 2014). The significant gradient between bay and ocean water levels after passing of a storm can scour previously deposited material and significantly affect the sediment budget of the beach-barrier-bay system due to this offshore sediment transport mechanism.

Storm surge at FI reached a peak storm elevation of 2.6 m NAVD88, which exceeded the 100-year high water level. This peak was preceded by a forerunner surge of about 1 m beginning approximately 18 hours before landfall, after which the water level steadily rose to 2.2 m NAVD88 over the next 12 hours. This flooded Christmas Bay and the back barrier region well before Ike made landfall. Waves offshore of FI exceeded 4.5 m significant wave height at 16 second peak period; roughly the 40-year wave conditions. After landfall, the water level quickly dropped to 2 m NAVD88 over the course of 12 hours. The amount of inland flooding from the forerunner resulted in a strong ebb flow that scoured large channels in FI as the water dragged sediment back out to the gulf.

The UTC is characterized by a series of long, narrow barrier islands and barrier peninsulas comprised of fine sand, and a microtidal, wave-dominated hydrodynamic environment (Morton et al., 1994; Mason, 1981). FI is one of the most vulnerable stretches of the UTC due to its lack of a major sediment source and high background erosion rates (Paine et al., 2012). The island is approximately 25 km long, less than 500 m wide and 2.06 m in elevation (NAVD88), and contains a series of beach communities, including Treasure Island and Surfside. In addition, FI protects important economic and ecological assets like Christmas Bay, the Brazoria National Wildlife Refuge, the CR-257 Blue Water Highway, the Gulf Intracoastal Waterway (GIWW), and parts of

the port of Freeport including the Naval Petroleum Reserve and an LNG de-liquification plant (Figure 4.1).

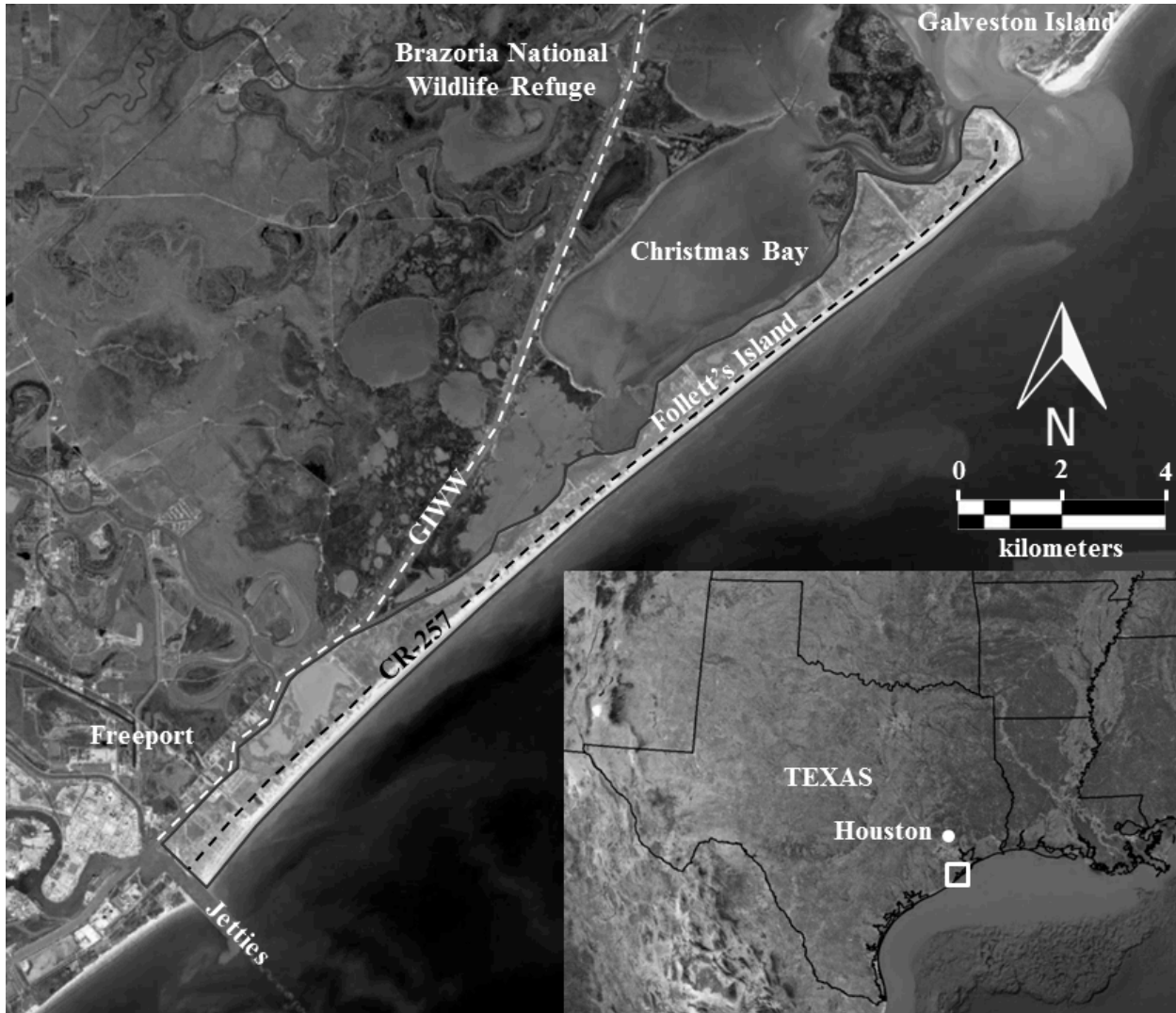


Fig. 4.1. Follet's island area map showing important economic assets such as the Port of Freeport and the Gulf Intracoastal Waterway (GIWW), and the CR-257 highway as well as ecological assets like Christmas Bay and the Brazoria National Wildlife Refuge.

In 1929, the Brazos River was rerouted 10.4 km (6.5 miles) west of the Freeport jetties. The Brazos River was formerly a major sediment source for FI, and its rerouting in conjunction with damming upriver resulted in a sediment deficit on FI (Morton and Pieper, 1975; Mason, 1981). As a result, FI experiences high rates of background erosion, with shoreline retreat between -1.5 m/yr and -3.9 m/yr (Paine et al., 2012).

In this study we observe the impact of the hurricane on the subaerial morphology of FI comparing results from the coastal response numerical models, XBeach and CSHORE (Roelvink,

2009; Johnson et al., 2012). While both numerical models utilize process-based techniques to compute short-term beach and dune morphology evolution, the two approaches differ greatly from each other.

4.3 Numerical Models

4.3.1 XBeach Background

XBeach is a powerful numerical modeling tool developed for modeling the coastal response of sandy beach systems to time-varying storm conditions (Roelvink, 2009). The model was built to simulate physical processes within different regimes of a storm as defined by Sallenger (2000) : (1) swash regime, (2) collision regime, (3) overwash regime, (4) inundation regime. For resolving swash dynamics, the model incorporates a 2DH description of wave groups from the time-varying wave action balance. This wave-group forcing drives infragravity (IG) motions, including both longshore and cross-shore currents. In the collision regime, an avalanching model is used to transport sediment from the dune face (dry) to the swash zone (wet), incorporating the fact that saturated sand moves more readily than dry sand. This is achieved by identifying a critical slope for both wet and dry conditions. For the overwash regime, wave group forcing of low frequency motions are applied with a robust momentum-conserving drying/flooding formulation and sediment transport formulation. Finally, the inundation regime includes a semi-empirical model for breach evolution based on a schematic uniform cross-section.

XBeach includes routines for short-wave envelope propagation (refraction and shoaling), non-stationary shallow water equations, undertow, and non-cohesive sediment transport and bed update, including avalanching, dune erosion, overwash, and breaching. The model includes a time-dependent wave action balance solver, eliminating the need for a separate wave model and allowing different wave groups to travel in different directions. The wave action balance is defined as:

$$\frac{\partial A}{\partial t} + \frac{\partial c_x A}{\partial x} + \frac{\partial c_y A}{\partial y} + \frac{\partial c_\theta A}{\partial \theta} = -\frac{D_w}{\sigma} \quad (1)$$

where the wave action, A , is defined by:

$$A(x, y, t, \theta) = \frac{S_w(x, y, t, \theta)}{\sigma(x, y, t)} \quad (2)$$

and where S_w represents the wave energy density in each directional bin, ϑ represents the angle of incidence with respect to the x-axis, σ represents the intrinsic wave frequency, D_w represents the wave energy dissipation, and c_x , c_y , and c_ϑ represent the wave action propagation speeds in x-, y-, and θ - space respectively.

The roller energy balance is coupled to the wave action balance based on the wave energy dissipation, D_w , and is defined as:

$$\frac{\partial S_r}{\partial t} + \frac{\partial c_x S_r}{\partial x} + \frac{\partial c_y S_r}{\partial y} + \frac{\partial c_\theta S_r}{\partial \theta} = -D_r + D_w \quad (3)$$

where $S_r(x,y,t,\vartheta)$ represents the roller energy in each directional bin, and D_r represents the total roller energy. Radiation stresses from the roller energy balance and the wave action balance are added together to calculate the radiation stress tensor used in the shallow water equation solver. For low frequency and mean flows, the shallow water equations are built into a depth-averaged Generalized Lagrangian Mean (GLM) formulation. These equations are based on the Lagrangian velocity, which in this context is equivalent to the Eulerian velocity plus the Stokes drift. The equations are summarized as:

$$\frac{\partial u^L}{\partial t} + u^L \frac{\partial u^L}{\partial x} + v^L \frac{\partial u^L}{\partial y} - f v^L - v_h \left(\frac{\partial^2 u^L}{\partial x^2} + \frac{\partial^2 u^L}{\partial y^2} \right) = \frac{\tau_{sx}}{\rho h} - \frac{\tau_{bx}^E}{\rho h} - g \frac{\partial \eta}{\partial x} + \frac{F_x}{\rho h} \quad (4)$$

$$\frac{\partial v^L}{\partial t} + u^L \frac{\partial v^L}{\partial x} + v^L \frac{\partial v^L}{\partial y} - f u^L - v_h \left(\frac{\partial^2 v^L}{\partial x^2} + \frac{\partial^2 v^L}{\partial y^2} \right) = \frac{\tau_{sy}}{\rho h} - \frac{\tau_{by}^E}{\rho h} - g \frac{\partial \eta}{\partial y} + \frac{F_y}{\rho h} \quad (5)$$

$$\frac{\partial \eta}{\partial t} + \frac{\partial h u^L}{\partial x} + \frac{\partial h v^L}{\partial y} = 0 \quad (6)$$

where u^L, v^L are Lagrangian velocities, f is the Coriolis coefficient, v_h is the horizontal eddy viscosity, h is the local water depth, τ_{bx}^E, τ_{by}^E are the Eulerian bed shear stresses, η is the water level, and F_x, F_y are the radiation stress tensors (from wave action balance and roller energy balance).

XBeach solves the depth averaged 2DH advection-diffusion equation to produce transport

vectors that are then used to update the bathymetry:

$$\frac{\partial hC}{\partial t} + \frac{\partial hCu^E}{\partial x} + \frac{\partial hCv^E}{\partial y} + \frac{\partial}{\partial x} \left[D_d h \frac{\partial C}{\partial x} \right] + \frac{\partial}{\partial y} \left[D_d h \frac{\partial C}{\partial y} \right] = \frac{hC_{eq} - hC}{T_s} \quad (7)$$

where C represents the depth averaged sediment concentration, u^E , v^E are Eulerian mean velocities, D_d is the sediment diffusion coefficient, and T_s is a modified time scale based on sediment fall velocity and local water depth. These formulations rely on the non-hydrostatic calculation of the wave group envelope and accompanying IG waves (including bound, free and trapped long waves). Infragravity waves make a significant contribution to shoreline erosion during storms, since a large portion of the offshore suspended sediment transport occurs at IG frequencies (Masselink, 1995).

In (8) and (9), the equilibrium sediment concentration C_{eq} is calculated using the Soulsby-Van Rijn transport formulation (Soulsby, 1997):

$$C_{eq} = \frac{A_{sb} + A_{ss}}{h} \left(\sqrt{u_{stirring}^2} - u_{cr} \right)^{2.4} (1 - \alpha_b m) \quad (8)$$

$$u_{stirring} = \sqrt{(u^E)^2 + (v^E)^2} + 0.018 \frac{u_{rms}^2}{C_d} \quad (9)$$

where A_{sb} and A_{ss} are bed and suspended load coefficients respectively, $u_{stirring}$ is the Soulsby-Van Rijn stirring velocity, u^E , v^E are Eulerian velocities, u_{rms} is the RMS bottom orbital velocity from wave action, C_d is the drag coefficient, u_{cr} is the threshold current speed (from Van Rijn method), α_b is a calibration factor and m is the bed slope (Soulsby, 1997). Here A_{sb} and A_{ss} are functions of the median sediment grain size (D_{50}), the ratio of densities of sediment grains to water, and the water depth. Furthermore, u_{cr} is a function of D_{50} , the 90th percentile grain size D_{90} , and the local water depth.

Finally, the bed level is updated based on gradients in sediment transport rates:

$$\frac{\partial z_b}{\partial t} + \frac{f_{mor}}{(1-p)} \left(\frac{\partial q_x}{\partial x} + \frac{\partial q_y}{\partial y} \right) = 0 \quad (10)$$

where z_b is the bed level, f_{mor} is a morphological acceleration factor, p is the sediment porosity,

and q_x and q_y are sediment transport rates in the cross-shore and alongshore directions respectively.

4.3.2 CSHORE Background

CSHORE is a very efficient 1D cross-shore coastal response model. The model includes a time-averaged and depth-averaged combined wave and cross-shore current model, a time-averaged sediment transport model, a probabilistic model for an intermittently wet and dry zone, as well as empirical formulas for irregular wave runoff (Johnson et al., 2012; Kobayashi et al., 2008). The model employs a linear wave theory based model below mean sea level (MSL) that merges with a non-linear shallow water model in the wet and dry zone. A more robust 2D version of the model, C2SHORE, is currently under development, and the following model formulations include longshore gradients that are neglected in the applied version of CSHORE.

The wave and current model is based on the time-averaged continuity and momentum equations (11-13), the wave action equation (14), and the roller energy equation (15).

$$\frac{\partial}{\partial x}(Q_x) + \frac{\partial}{\partial y}(Q_y) = 0 \quad (11)$$

$$\frac{\partial}{\partial x}\left(\frac{Q_x^2}{\bar{h}}\right) + \frac{\partial}{\partial y}\left(\frac{Q_x Q_y}{\bar{h}}\right) + g\bar{h}\frac{\partial \bar{\eta}}{\partial x} + \frac{\tau_{bx}}{\rho} = \tau_{wx} + \frac{\tau_{sx}}{\rho} \quad (12)$$

$$\frac{\partial}{\partial x}\left(\frac{Q_x Q_y}{\bar{h}}\right) + \frac{\partial}{\partial y}\left(\frac{Q_y^2}{\bar{h}}\right) + g\bar{h}\frac{\partial \bar{\eta}}{\partial y} + \frac{\tau_{by}}{\rho} = \tau_{wy} + \frac{\tau_{sy}}{\rho} \quad (13)$$

where Q_x , Q_y are time-averaged volume fluxes, \bar{h} is the mean water depth, $\bar{\eta}$ is the wave setup, τ_{bx} , τ_{by} are bottom shear stresses, τ_{sx} , τ_{sy} are wind shear stresses on the water surface, and τ_{wx} , τ_{wy} are wave-induced shear stresses (estimated from the gradient in wave induced fluxes and radiation stresses). The wave action equation is expressed as:

$$\frac{\partial}{\partial x}\left[\frac{E}{\omega}\left(C_g \cos \theta + \frac{Q_x}{\bar{h}}\right)\right] + \frac{\partial}{\partial y}\left[\frac{E}{\omega}\left(C_g \sin \theta + \frac{Q_y}{\bar{h}}\right)\right] = -\frac{D_B - D_f}{\omega} \quad (14)$$

where E is the wave energy, ω is the intrinsic angular frequency, C_g is the group velocity, θ is the incident wave angle, and D_B , and D_f are dissipation rates due to wave breaking and bottom friction, respectively. The roller volume flux, q_r , is computed using the roller energy equation:

$$\frac{\partial}{\partial x}(\rho C^2 q_r \cos \theta) + \frac{\partial}{\partial y}(\rho C^2 q_r \sin \theta) = D_B - D_r \quad (15)$$

where C is the phase velocity, q_r is the roller volume flux, and D_r is the roller dissipation rate. This model calculates cross-shore variations of the mean and standard deviation of the free surface elevation as well as the depth-averaged cross-shore and longshore velocities. Since CSHORE is a 1D time-averaged model, it cannot accurately model areas with large alongshore bathymetric gradients; thus it is most effective when applied to a shore location where bathymetric contours are approximately parallel.

The sediment transport model included in CSHORE incorporates the hydrodynamic forcing to compute depth-averaged suspended sediment load and bed load. Suspended sediment volume is related to sediment fall velocity and the energy dissipation rates (14 and 15), and the suspended sediment transport rate is related to the undertow current and the horizontal cross-shore velocity. Bed load transport rate depends on the standard deviation of the depth-averaged horizontal velocity. Incipient mobilization of sediment is calculated using a critical Shields parameter (ψ_c) of 0.05. The net cross-shore sediment transport rate is the sum of the net bed load and suspended sediment transport rates.

This model is limited to globally uniform sediment parameters characterized by the median diameter (D_{50}), the fall velocity (w_f), and the specific gravity (s). The probabilistic model for the wet and dry zone was calibrated and verified by the developers using small-scale lab tests (e.g. Kobayashi et al., 2008; Figlus et al., 2011). This model is used to predict wave overwash and structural damage progression. One weakness of CSHORE is that in its current state it cannot calculate offshore sediment transport due to storm surge ebb, which is a major contributor to the response of FI to Hurricane Ike. However, it is expected that the initial morphodynamic response to the storm can be simulated.

4.3.3 Model Setup

4.3.4 Boundary Conditions

To ensure accurate hydrodynamic forcing conditions for the numerical models XBeach and CSHORE, continuous time series of wave and water level parameters are required at or near the model boundary. Since recorded data in the vicinity of FI are limited, the continuous boundary conditions must be extracted from large-scale numerical modeling results that simulate the hydrodynamics of Hurricane Ike. For this, two potential parent simulations were considered: (1) Coastal Storm Modeling System (CSTORM) model results produced by the USACE Engineer Research and Development Center (ERDC), and (2) ADCIRC+SWAN model results provided by Dr. Casey Dietrich of North Carolina State University (Hope et al., 2013).

The time series of water surface elevation in the nearshore region of FI was characterized by two peaks occurring roughly 11 hours apart. The first peak, which occurred on the evening of Sep-12, was resultant of the forerunner surge and can be attributed to Ekman setup (Kennedy et al., 2011). The second peak, which occurred on the morning of Sep-13, was resultant of the hurricane storm surge. In the nearshore region, the storm surge peak was of greater magnitude than the forerunner surge. Both models slightly overestimate the storm surge peak WSEL by 0.2-0.4 m in the nearshore region, but underestimate the forerunner surge by up to one meter. Additionally, there was a resurgence wave of smaller magnitude occurring one day after the initial surge that was underestimated by about 1 m in both models. The timing of surge onset and retreat is accurately captured in the nearshore environment. In the nearshore, the ADCIRC+SWAN model does a slightly better job of simulating the forerunner surge, but the CSTORM model more accurately predicts the peak WSEL.

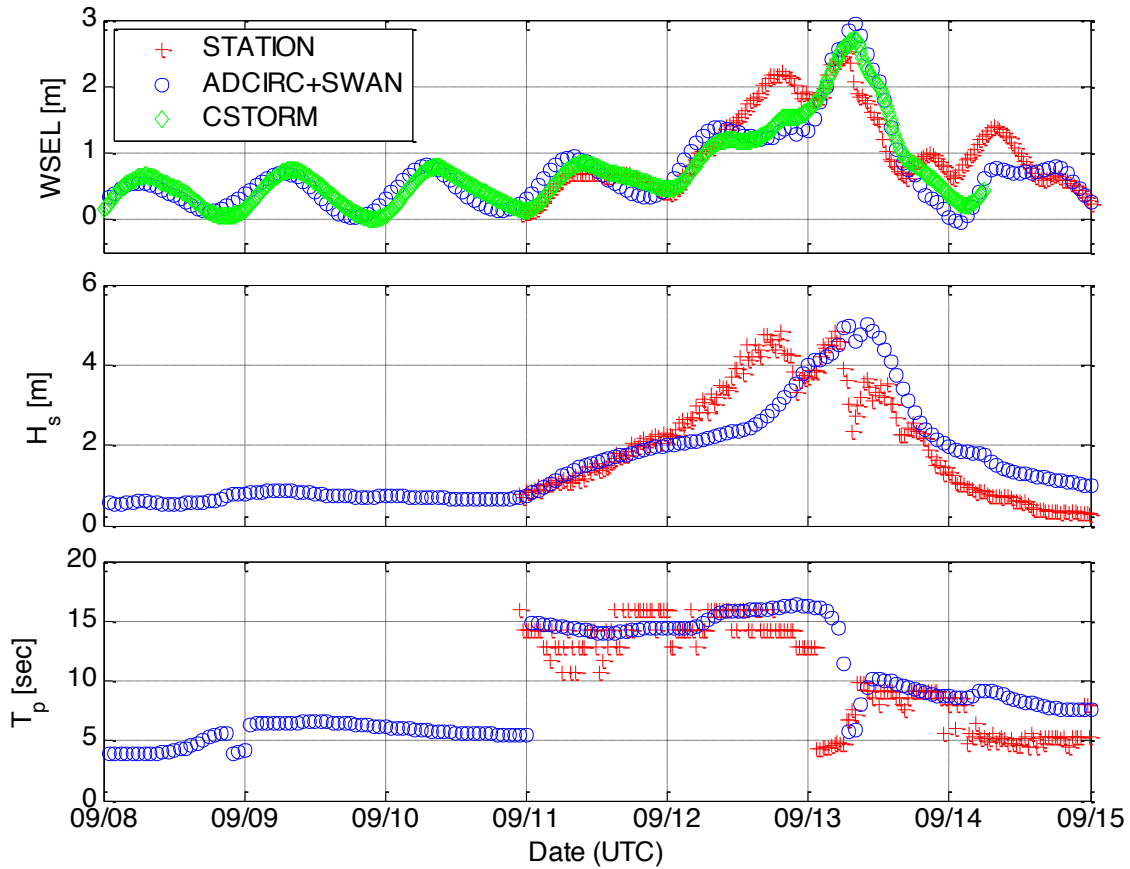


Fig. 4.2: Validation of modeled WSEL (top), H_s (middle) and T_p (bottom) at nearshore location: Kennedy Gauge W.

Figure 4.2 shows the validation of water surface elevation, significant wave height and peak period at a nearshore location from Kennedy Gauge W. The validation of wave parameters was limited to the ADCIRC+SWAN in this study. In the nearshore, maximum wave heights were accurately captured to within 0.3 m. The timing of wave onset matched recorded data, however the time of maximum wave height lagged behind observations by approximately 15 hours.

In summary, both models are able to accurately capture maximum wave and water level conditions. However, significant wave heights and water levels tend to lag by 12-15 hours. In the absence of a better alternative, either one of these models are acceptable for providing boundary conditions to the coastal response models, especially since the time lag was relatively consistent for both water surface and wave parameters. Since simulation results from both models were fairly consistent, the ADCIRC+SWAN simulation was chosen as the parent model because these data were more accessible than the CSTORM data.

4.3.5 Grid Generation

XBeach uses a 2D-rectilinear grid with variable grid spacing in both x- and y-directions. The model grid is oriented with the positive x-direction onshore and positive y-direction alongshore, with the grid origin at the lower left corner at the offshore boundary. This orientation allows the variable x-resolution to efficiently resolve cross-shore features like the foredune.

The variable cross-shore resolution can be calculated automatically using a specified Courant condition of 0.7 with the maximum offshore boundary resolution calculated based on a minimum mean period and a user defined minimum dry land resolution. This method created an unreasonably small cross-shore resolution in the back-bay (where wave action is expected to be minimal). Thus, the cross-shore resolution of the back bay was adjusted to 20 m to minimize computational expense. The final cross-shore resolution varied between 20 m at the offshore and back bay boundaries and 5 m at the shoreline.

The final grid encompassed all of FI from approximately 2.5 km offshore to half way through Christmas Bay (Fig. 4.3). The lateral extent was from the west end of Galveston Island to the Freeport Jetties. This region originally had an average elevation of 2 m NAVD88.

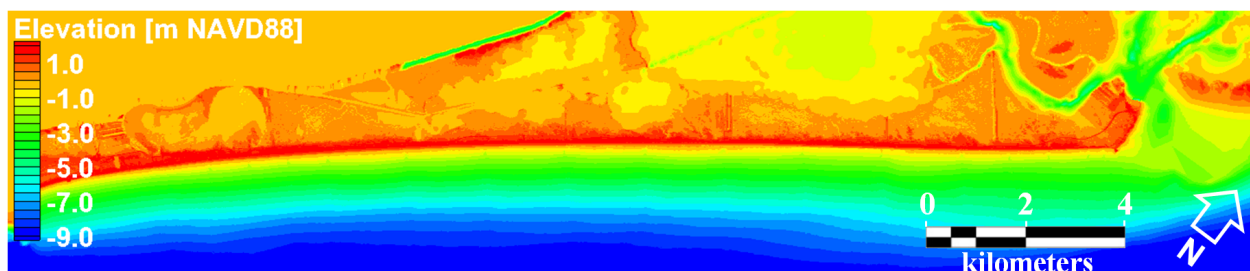


Fig. 4.3: Bounds and relief of the XBeach model grid.

CSHORE runs on 1-D cross-shore bathymetric profiles that are oriented positive shoreward with the origin at the offshore boundary. These profiles were extracted along eight survey transects (Fig. 4.4). The model domain was truncated at highway CR-257 to maintain consistency with the analysis of LiDAR data. CSHORE requires that the prescribed surge level never exceed the highest bed level in the domain.

4.3.6 Numerical Model Setup

For the XBeach simulation, time histories of water surface elevations from the parent model SWAN+ADCIRC were extracted at the four corners of the model domain. Water surface boundary conditions were applied at the corners of the model domain and were interpolated

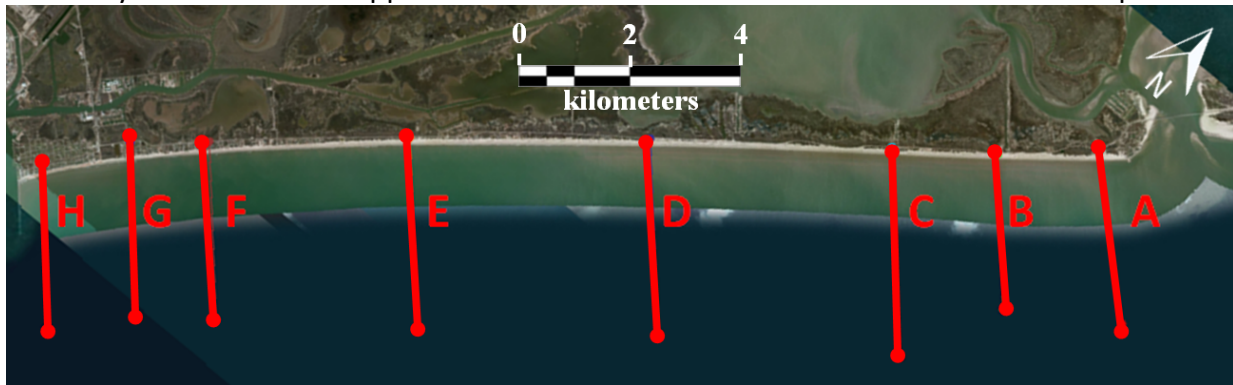


Fig. 4.4: Cross-shore transects for analysis of island topography and bathymetry

spatially along the boundary edges. The time steps of the water surface boundary conditions were also linearly interpolated onto the model time step, meaning that the input temporal resolution of water surface can be large as long as it accurately resolves storm surge.

Time histories of significant wave height, peak wave period and mean wave direction were extracted from the parent model at the offshore boundary of the XBeach grid. The time steps of wave parameters were linearly interpolated onto the model time step. Thus, the input wave parameter time step needs to be only small enough to resolve the bound long waves.

XBeach is a computationally intensive model, and as an option to reduce the run time, a morphological acceleration (morfac) scheme was built into the code (10). This allows the possibility of artificially reducing the total model time by accelerating hydrodynamic forcing and compounding sediment transport rates by some factor. In other words, the morphological time scale is sped up by some prescribed factor relative to the hydrodynamic time scale. Lindemer et al. (2010) and McCall et al. (2010) performed sensitivity analyses of the morphological acceleration parameter and concluded that for values between 1 and 20, there was less than 2% difference in the resulting coastal response, despite a significant reduction in the computation time. Thus a morfac value of 10 was chosen for the base simulation.

McCall (2008) determined that XBeach will tend to over predict the morphological change associated with sheet flow, such as during the inundation regime. Thus, XBeach has a built-in trigger to artificially limit the maximum Shields number to a constant value, with recommended values between 0.8 and 1.2 (Eq. 16).

$$u_{stirring}^2 = \min \left(u_{stirring}^2, \theta_{sf} \frac{g D_{50} \Delta}{c_f} \right) \quad (16)$$

where $u_{stirring}$ is the Soulsby-Van Rijn stirring velocity during sheet flow (9), θ_{sf} is the threshold Shields parameter for the start of sheet flow (denoted as s_{max} in the XBeach model input), D_{50} is the median sediment grain size, and Δ is the relative density of the sediment. This method assumes that during sheet flow, higher velocities correspond to higher transport rates, but not to higher equilibrium sediment concentrations.

Table 4.1: Xbeach smax sensitivity testing on Section A. Total eroded and accreted sediment volume in XBeach with varying smax values.

| smax | Computation time [min.] | Total Accreted [m ³ /m] | Volume Eroded [m ³ /m] |
|----------|-------------------------|------------------------------------|-----------------------------------|
| No Limit | 4.9 | 3.10 | -35.87 |
| 1.2 | 5.0 | 10.58 | -17.02 |
| 1.0 | 4.8 | 10.44 | -14.17 |
| 0.8 | 4.8 | 9.14 | -11.26 |

A sensitivity test was conducted on the s_{max} factor to test how varying this parameter affects the final bed elevation Figure 4.5 compares the final bed elevation with s_{max} values from 0.8 to 1.2. A summary of the eroded and accreted volumes from these results is shown in Table 4.1. It is clear that specifying a higher maximum Shields number leads to a greater magnitude of bed level change. An s_{max} value of 0.8 was chosen for the base simulation.

The additional free parameters contained in XBeach that govern model numerical schemes, breaker parameters, critical avalanching slopes, etc. were all left at their default values.

For the CSHORE model, time histories of water surface elevation, significant wave height, peak wave period, and mean wave direction were extracted from the parent model SWAN+ADCIRC at the offshore boundary of each profile. Wave incident angles at the offshore boundary were converted relative to shore-normal. The models were run for a total model time of 96 hours beginning Sep-10, 2008 15:00 GMT.

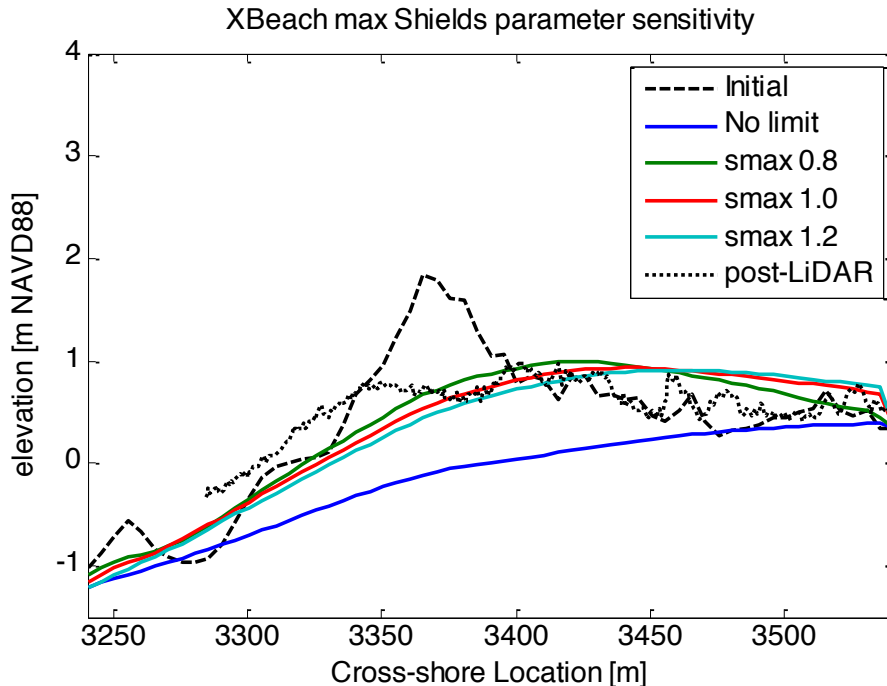


Fig. 4.5: Final land surface elevation comparison from XBeach model with varying s_{max} values. Simulation was run in 1-D mode on cross-shore Section A.

4.4 Model Outcomes

4.4.1 XBeach Results

The XBeach simulation clearly captures processes involved in the collision, overwash, and inundation regimes outlined by Sallenger (2000). In addition to these regimes, it is clear that storm surge ebb plays a large role in transporting sediment offshore, a phenomenon also recognized by Goff et al. (2010) and Hayes (1967). Figure 4.6 shows snapshot images from an approximately 2 km long by 1 km wide portion of the model domain during the collision regime, overtopping regime, inundation regime, and during storm surge ebb.

From hours 32 to 52, FI was in the overtopping regime, during which time the foredune crest elevation was lowered slightly in some areas as wave runup washed sediment from the lower elevation dunes to the back barrier. During this regime, the morphological response was mostly limited to the dune and immediate back-barrier where dune overwash sediments were deposited just landward of the foredune. Beach erosion during this regime was minimal.

From hours 52 to 62, FI experienced massive erosion of the foredune during the inundation regime. In the hours leading up to landfall, the storm surge spiked rapidly and the foredune, which had already been lowered slightly during the overwash regime, was uniformly inundated

causing a large volume of sediment to be transported from the foredune to the back barrier and back bay. During this regime, wave action was minimal and the sheet flow from the surge gradient dominated the sediment transport process.

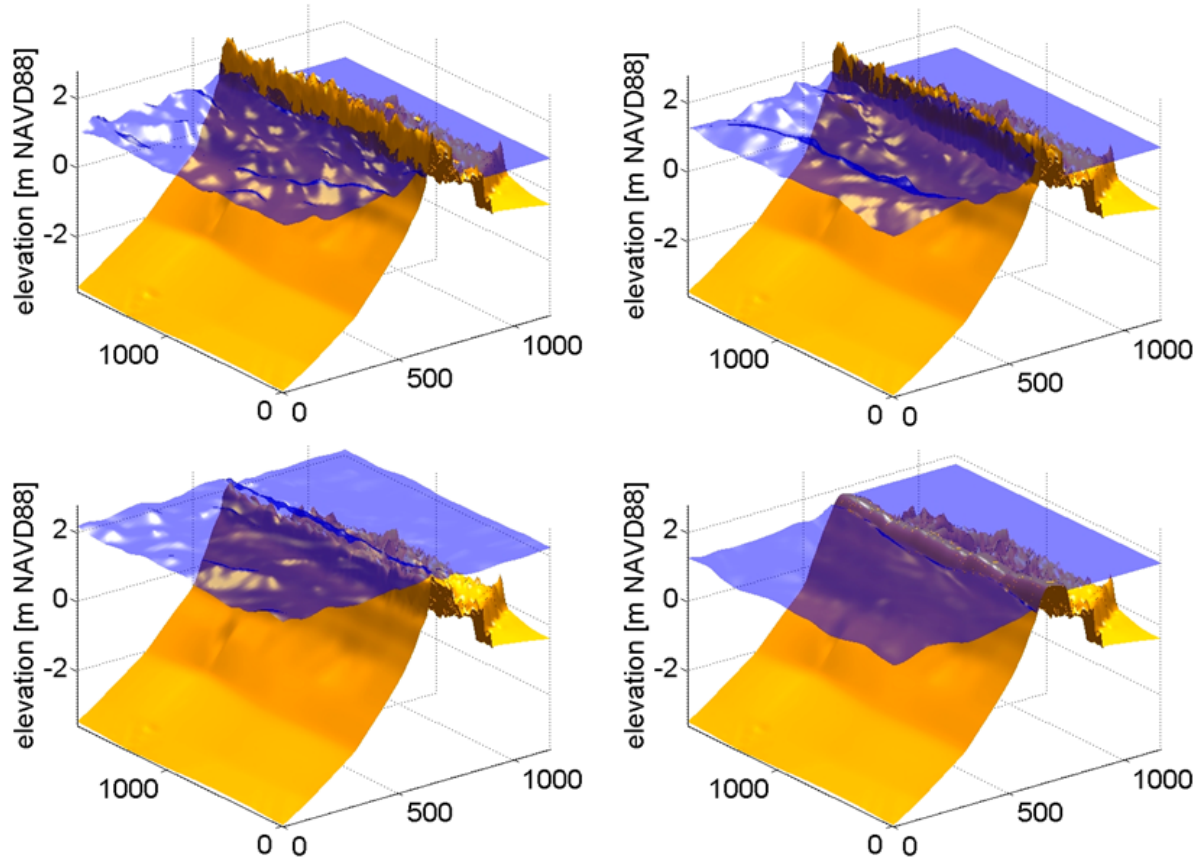


Fig. 4.6: Snapshot of water surface (long waves only) and bed level during the collision regime (top-left), during the overtopping regime (top-right), during the inundation regime (bottom-left), and during storm surge ebb (bottom-right).

From hours 62 to 73, high velocities from the ebbing storm surge pulled large volumes of sediment offshore, further flattening and lowering the beach and steepening the subaqueous shoreface. After the storm surge ebb, the island experienced a resurgence wave; however this wave was not large enough to overtop the island a second time. This resurgence wave had minimal impact on the shoreface, but did raise the forebeach elevation slightly.

Figure 4.7 outlines each impact regime and the associated hydrodynamics and morphological response. The volume changes associated with each impact regime are shown in Table 4.2. It is clear from this table that the total accreted and eroded sediment volume increased by nearly 60% during the 10 hour inundation regime. During this time the accretion and erosion rates were 50 - 100% higher than during any other regime. During the 11 hours storm surge ebb

regime, the rates of erosion and accretion were about half those during the inundation regime but still about 50% higher than during the other regimes.

Simulated post-storm bed level profiles were compared with post-storm LiDAR profiles along the cross-shore transects shown in Figure 4.4. Sample profiles from Section A and Section D are shown in Figure 4.8. It is clear from this figure that the overwash regime had a much more significant impact on Section A than on Section D. This is likely due to the fact that the initial dune crest elevation at Section A was approximately 50 cm lower than at Section D. Furthermore, due to the lower elevation on the east end of the island, the resurgence wave had a much greater impact on Section A than any of the other sections. Here the shoreline was extended farther offshore between hours 73 and 96, where the other areas experienced little impact.

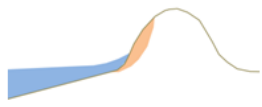
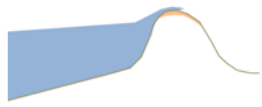


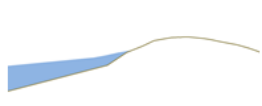
| | Time [hrs] | Hydrodynamic characteristics | Morphological Response | Schematic |
|------------|------------|---|--|---|
| Collision | 0 - 32 | Wave runup attacks the dune face. | Sediments from the dune toe and dune face are pulled offshore. |  |
| Overwash | 32-52 | Wave runup level exceeds the dune crest. | Sediments from the dune crest are washed over to the back barrier. |  |
| Inundation | 52-62 | Surge level exceeds the dune crest. | Significant washover of dune sediments to the back barrier. |  |
| Ebb | 52-73 | Storm surge recedes and flows back to the ocean | Sediment is dragged back offshore creating scour channels. |  |
| End | 73-96 | Surge has completely receded and waves dominate the hydrodynamics | Minimal morphological response |  |

Fig. 4.7: Outline of Hurricane Ike storm impact regimes on Follet’s Island based on numerical modelling results.

The XBeach simulation was able to capture the large-scale 2D erosional patterns of the island. The locations of two significant breaches were accurately reproduced with XBeach (Fig. 4.9).

Both of these locations initially had a relatively low and narrow foredune, and thus were particularly susceptible to breaching. Although the large-scale erosion trends are accurately simulated in XBeach, it is clear that the small-scale erosion patterns (such as the specific ebb channels) are not accurately reproduced. This is likely due to the influence of structures, vegetation, and spatially variable geology that are not included in the XBeach model.

Table 4.2: XBeach simulated volume of subaerial accretion and erosion at the end of the collision regime (32 hrs.), the overwash regime (52 hrs.), the inundation regime (62 hrs.), the storm surge ebb (73 hrs.), and at the end of the model (96 hrs.).

| | Volume accreted [m ³] | Accretion rate [m ³ /hr] | Volume eroded [m ³] | Erosion rate [m ³ /hr] | Net volume change [m ³] |
|---------|-----------------------------------|-------------------------------------|---------------------------------|-----------------------------------|-------------------------------------|
| 32 hrs. | +359,252 | +11,226 | -325,601 | -10,175 | +33,651 |
| 52 hrs. | +598,407 | +11,957 | -519,788 | -9,709 | +78,618 |
| 62 hrs. | +914,301 | +31,589 | -820,441 | -30,065 | +93,860 |
| 73 hrs. | +1,103,664 | +17,214 | -1,055,741 | -21,390 | +47,923 |
| 96 hrs. | +1,181,603 | +3,388 | -1,147,824 | -4,003 | +33,779 |
| LiDAR | +1,430,593 | | -833,440 | | +597,153 |

One way to quantify the accuracy of a model is to compare the error in modeled bed level change to the variance of the observed bed level change from LiDAR data; known as the simulation skill (17). It is also important to calculate the mean error in the simulation to determine whether the simulation errors are due to random differences in bed elevation or due to a general trend; known as the simulation bias (18). Since these values can only be computed in areas where data sources overlap, the calculations are limited to the subaerial beach where LiDAR surveys are available (McCall et al., 2010).

$$Skill = 1 - \frac{\sum_{i=1}^N (dz_{b_{LiDAR,i}} - dz_{b_{Model,i}})^2}{\sum_{i=1}^N (dz_{b_{LiDAR,i}})^2} \quad (17)$$

$$Bias = \frac{1}{N} \sum_{i=1}^N \left(z_{b_{post-storm,Model,i}} - z_{b_{post-storm,LIDAR,i}} \right) \quad (18)$$

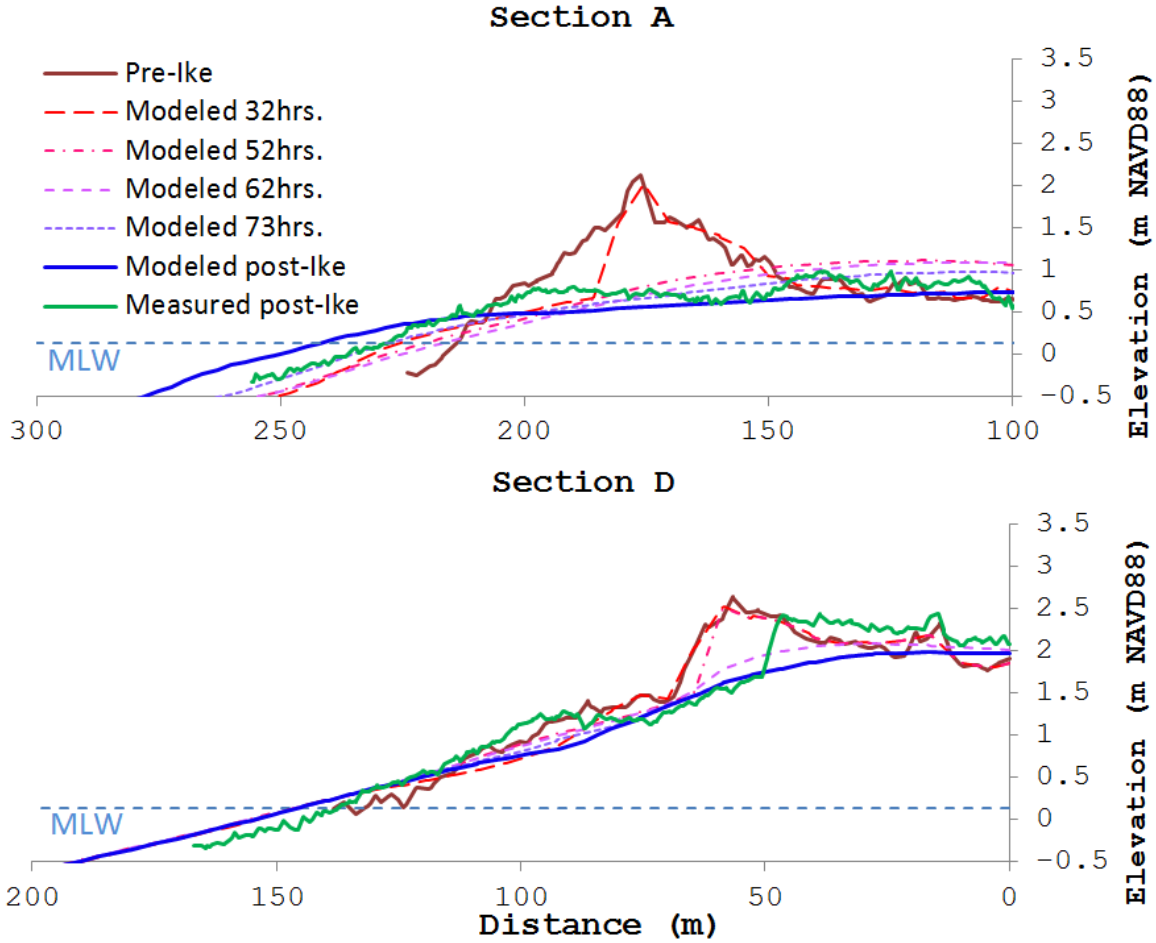


Fig. 4.8: XBeach simulated bed level evolution compared to pre- and post-storm bed level extracted from LiDAR data at Sections A (the west end of FI) and Section D (near the center of Follet's Island).

where N is the total number of grid points in the overlapping coverage area, $dz_{b_{Model,i}}$ is the measured bed level change at point i , and $dz_{b_{LIDAR,i}}$ is the modeled bed level change at point i . If the skill is equal to one, then the simulation perfectly predicts the bed level change. If the skill is zero, then the simulation is no more accurate than predicting zero bed level change. If the skill is less than zero, then the simulation is less accurate than predicting zero bed level change. Furthermore, a positive bias means the model has predicted a higher post-storm bed elevation

than is observed, and a negative bias means the model has predicted a lower post-storm bed elevation.

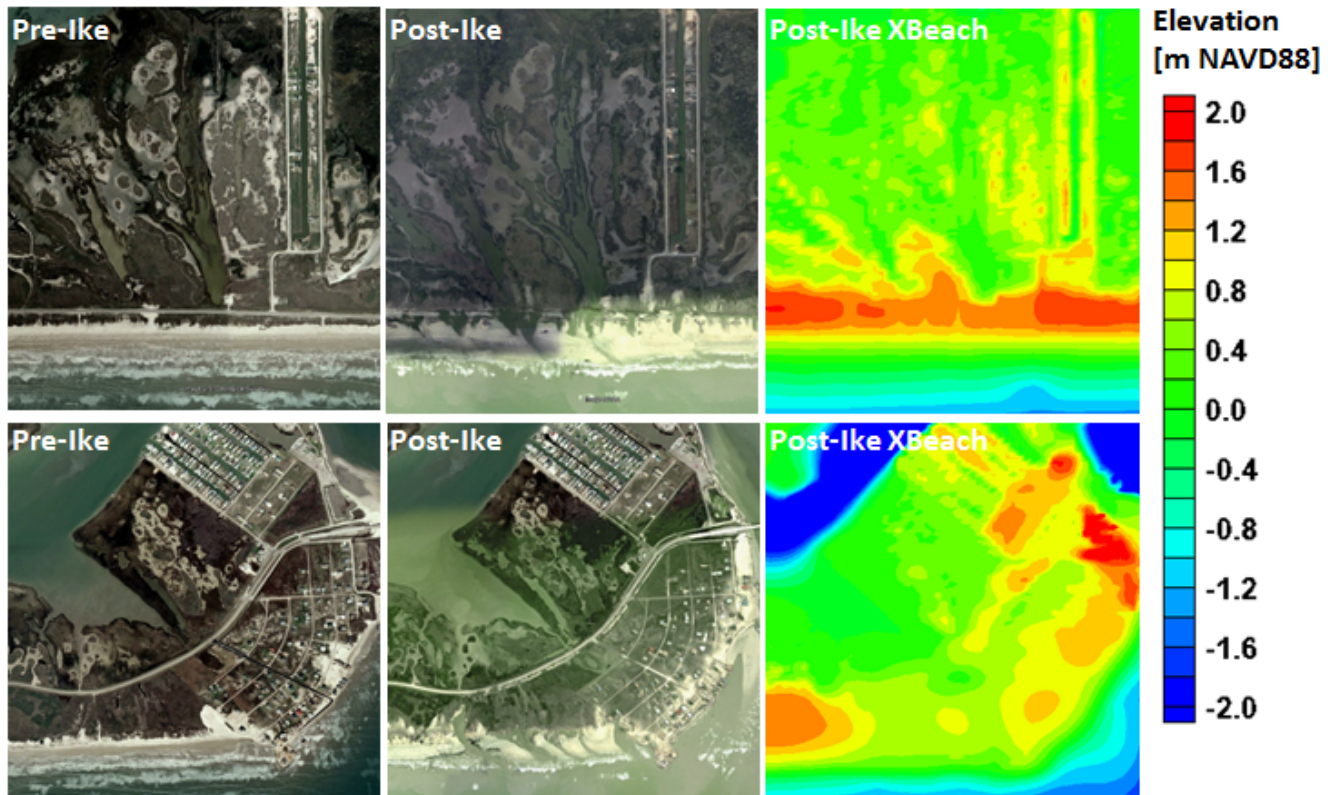
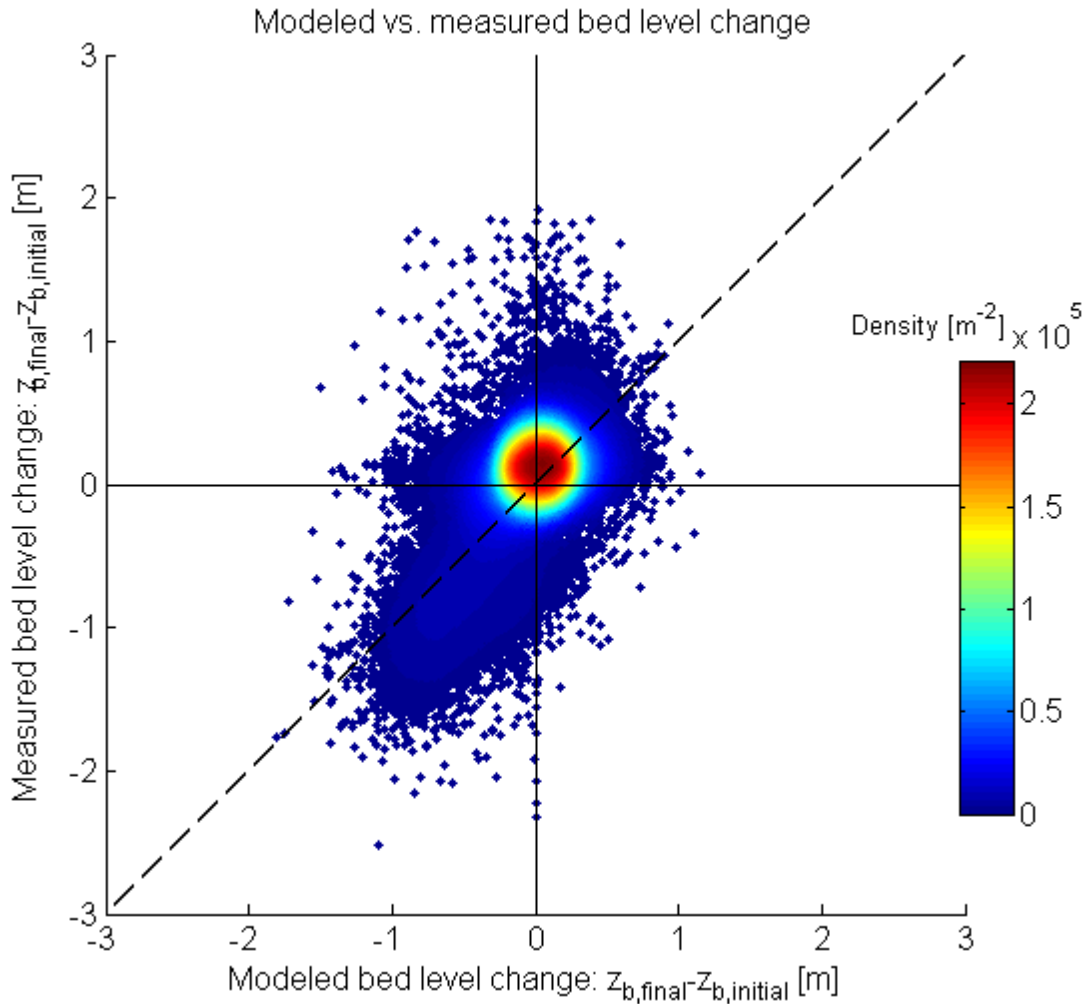


Fig. 9: XBeach simulated erosion trends compared with LiDAR observations.

Based on (17) and (18) the skill of this XBeach simulation is 0.35 with an overall bias of -0.06. This is considerably lower than the skill of 0.74 from a similar study by McCall et al. (2010). There are a number of factors that could contribute to this. Where the study by McCall et al. focused on a mostly unvegetated stretch of island, the back barrier of FI is abundantly covered with grass, which cannot be included in the current build of XBeach. De Vet et al. (2015) has attempted to include the effects of vegetation on coastal response with some success by using a spatially variable Manning's roughness coefficient. However this method still requires some testing to confirm its accuracy at modelling the impact of vegetation. In addition to the influence of vegetation, there are likely errors in the computed difference in the LiDAR surveys from the filtering of buildings and foliage, which was performed by deleting any areas that showed a net gain in land surface that exceeded two meters; the assumption being that a greater than two meter net rise in bed level is unrealistic and thus represents the existence of buildings or foliage.

The skill of this simulation is shown graphically in Figure 4.10, where the measured bed level change is plotted relative to the modeled bed level change. The color scale in this plot represents the point density in points per square meter. It is clear from Figure 4.10 that the

greatest density of measured bed change was between -5 cm and +30cm. Based on this figure, XBeach had a tendency to underestimate both accretional and erosional bed level change. There is also a cluster of points of measured bed level change greater than 1 m that were significantly



underestimated by XBeach. It is likely that these points are associated with the difference in LiDAR returns between the pre- and post-ike surveys that were not filtered out.

Fig. 10: Measured bed level change vs. modeled bed level change for all grid points in overlapping coverage area. The dashed line represents a perfect 1:1 relation. Color scale indicates point density in points per square meter. Positive values represent accretion and negative values represent erosion.

4.4.2 CSHORE Results

CSHORE was run separately for the eight different bed profiles associated with Sections A-H (Fig. 4.4). During the collision regime, the foredune, beach, and foreshore experience only minimal bed level change. During the overwash regime, the wave runup exceeds the dune crest causing washover of dune sediments and slight lowering of the dune crest (0.1 – 0.6 m). During the inundation regime, the beach is flattened and the shoreline is extended seaward while the dune is drastically lowered in elevation and pushed landward. There is very little bed level change associated with storm surge ebb and the resurgence wave since CSHORE does not model offshore directed return flow in its current build and the resurgence wave is not large enough to cause major morphological changes.

Table 4.3 summarizes the volume accreted and eroded at the end of each regime. The bulk of the bed level change is associated with the overwash and inundation regimes. Erosion rates during the inundation regime are still higher than any other regime, but not proportionally as high as in the XBeach model. Also unlike the XBeach model, the storm surge ebb regime does not have a significant impact on the total bed level change. This is understandable, as the hydrodynamics associated with the ebbing storm surge are not built into the time-averaged CSHORE model.

Table 3: CSHORE simulated volume of accretion and erosion at Section-D at the end of the collision regime (32 hrs.), the overwash regime (52 hrs.), the inundation regime (62 hrs.), the storm surge ebb (73 hrs.), and at the end of the model (96 hrs.).

| | Volume accreted [m ³ /m] | Accretion rate [m ³ /m-hr] | Volume eroded [m ³ /m] | Erosion rate [m ³ /m-hr] | Net volume change [m ³ /m] |
|---------|-------------------------------------|---------------------------------------|-----------------------------------|-------------------------------------|---------------------------------------|
| 32 hrs. | +7.5 | +0.23 | -7.3 | -0.23 | +0.1 |
| 52 hrs. | +18.6 | +0.56 | -18.1 | -0.54 | +0.6 |
| 62 hrs. | +25.9 | +0.73 | -24.0 | -0.59 | +2.0 |
| 73 hrs. | +27.5 | +0.14 | -25.3 | -0.12 | +2.3 |
| 96 hrs. | +28.5 | +0.04 | -26.1 | -0.03 | +2.4 |

Simulated post-storm bed level profiles were compared with post-storm LiDAR profiles along Sections A-H (Fig. 4.5). Sample profiles from Section A and Section D are shown in Figure 4.11. Based on these figures it is clear that CSHORE very accurately predicts the post-storm beach slope and shoreline. However, CSHORE is less effective at predicting the morphology of the foredune. This is likely due to the fact that the dune morphodynamics is largely driven by sheet

flow associated with surge overtopping and inundation; a physical process that is not included in the CSHORE model.

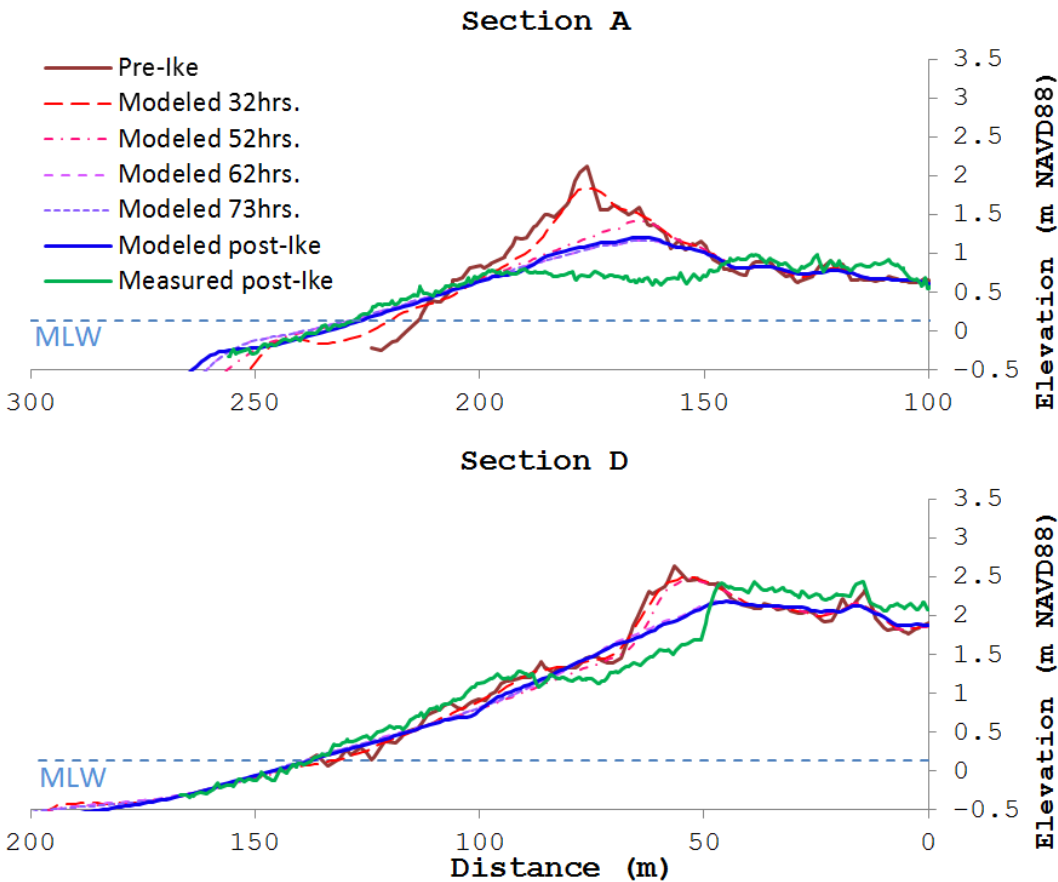


Fig. 11: CSHORE simulated bed level evolution compared to pre- and post-storm bed level extracted from LiDAR data at Sections A (the west end of FI) and Section D (near the center of Follet’s Island)

The skill and bias of the CSHORE simulations were calculated for each profile and these values are summarized in Table 4.4. Since Sections F-H are located on the more developed west end of the island, it is likely that anthropogenic influences contribute to the lower skill for these sections. Excluding Sections F-H, the skill becomes 0.408 and the bias 0.737. Sections B and C display a clear positive bias that is likely due to truncation of the domain at CR-257.

To compare the skill of CSHORE directly with that of XBeach, the skill of each model must be calculated over the same coverage area. Since the CSHORE calculation is limited to cross-shore transects, the skill and bias of XBeach on those same transects was calculated and shown in Table 4.4 for direct comparison with CSHORE results.

The total skill of the CSHORE simulations was 0.35, approximately the same as the total skill of the XBeach simulation. However, when evaluating the skill only on cross-shore Sections A-H, the skill of CSHORE was approximately 30% lower than Xbeach. In fact, on the east end of the island (Sections A & B), XBeach showed skill as high as 0.81. However, near the center and east end of the island, CSHORE had a higher skill than XBeach. This is likely due to the fact that the resilient vegetation in that region prevented the dune from being completely eroded. Thus, the fact that CSHORE inherently underpredicts the lowering of the dune during the inundation regime coincidentally results in a better skill score at Sections D-F.

Table 4.4: Skill and bias of CSHORE and XBeach simulations for Sections A-H.

| | CSHORE | | XBeach | |
|-----------|--------|----------|--------|----------|
| | Skill | Bias [m] | Skill | Bias [m] |
| Section A | 0.629 | 0.007 | 0.789 | 0.016 |
| Section B | 0.388 | 0.655 | 0.811 | 0.100 |
| Section C | 0.283 | 0.380 | 0.670 | -0.069 |
| Section D | 0.496 | -0.051 | 0.326 | -0.041 |
| Section E | 0.413 | -0.005 | -0.109 | -0.026 |
| Section F | 0.382 | -0.038 | -0.374 | -0.049 |
| Section G | 0.087 | -0.164 | -0.040 | -0.125 |
| Section H | -0.109 | -0.055 | 0.000 | 0.075 |
| Total | 0.345 | 0.170 | 0.491 | 0.002 |

4.5 Discussion and Conclusions

In this study, the morphodynamics of the subaerial portion of FI, a low-lying, sediment-starved barrier island on the Upper Texas Coast, were examined in response to hydrodynamic forcing conditions from Hurricane Ike. Hurricane Ike was one of the most destructive storms to ever hit the UTC. Although FI was on the western side of Ike’s eye at landfall and thus subject to predominantly offshore directed winds, the resulting storm surge overtopped and inundated the island. During this process, complex hydrodynamic forcing associated with ocean-to-bay directed overwash sheet flow and subsequent bay-to-ocean directed ebb sheet flow modified the morphology of FI drastically.

Based on the numerical modelling results, it is clear that both XBeach and CSHORE were able to reproduce the morphological response of FI to Hurricane Ike with varying degrees of skill. XBeach was more accurate at simulating the coastal response to the foredune and beach system, and was also able to capture 2D effects such as the locations of breaches. It includes model routines for calculating hydrodynamics and transport due to sheet flow; something that proved to be a major contributor to the overall response of the island. However, XBeach required a significantly longer run time than CSHORE, making it a less practical model choice for

simulating large numbers of storms or design scenarios in future coastal projects.

CSHORE was able to accurately calculate the post-storm slope and shoreline, however was less effective at simulating the response of the foredune. Furthermore, it does not include routines for sheet flow, making it an impractical model choice for scenarios where sheet flow is likely to be a major driver of the coastal response. CSHORE has further limitations on the model domain. In its current build, CSHORE is unable to simulate transport across a full cross-section of the island, from offshore to the back bay, and cannot capture 2D alongshore transport trends. Despite these limitations, CSHORE was able to simulate the response of FI with a skill as high as 0.61.

Both models show that the greatest change in bed level of FI was associated with the inundation regime of Hurricane Ike, which lasted only about 10 hours. During this regime, bed level change rates were up to three times greater than during the collision and overwash regimes. XBeach was also able to capture significant bed level change associated with storm surge ebb which corresponds with observations of multiple ebb flow channels that were scarped into the island after the passage of Hurricane Ike.

4.6 Acknowledgements

This project was supported in part by an Institutional Grant (NA14OAR4170102) to the Texas Sea Grant College Program from the National Sea Grant Office, National Oceanic and Atmospheric Administration, U.S. Department of Commerce. Additional funding was provided by the Texas General Land Office and NOAA through the Texas Coastal Management Program, Grant number 13-431-000-7890. Support during the data mining process was also provided by the Texas General Land Office and Coast & Harbor Engineering, a Division of Hatch-Mott McDonald. The authors would like to thank Dr. Casey Dietrich for providing the ADCIRC+SWAN model outputs used as the forcing conditions in this study.

4.7 References

- de Vet, P., & Lodewijk, M. (2015). Modelling dune erosion, overwash and breaching at Fire Island (NY) during Hurricane Sandy. *Proceedings of Coastal Sediments 2015, San Diego, CA*.
- Donnelly, C., Kraus, N., & Larson, M. (2016). State of knowledge on measurement and modeling of coastal overwash. *Journal of Coastal Research*, 22(4), 965–991.
- Figlus, J., Kobayashi, N., Gralher, C., & Iranzo, V. (2011). Wave Overtopping and Overwash of Dunes. *Journal of Waterway, Port, Coastal, and Ocean Engineering*, 137(1), 26–33.
- Gibeaut, J. (2011). *Changes along the Texas barrier island coast*. Presentation presented at the

Gulf Coast Ecosystem Restoration Task Force Meeting, Galveston, TX.

- Goff, J. A., Allison, M. A., & Gulick, S. P. S. (2010). Offshore transport of sediment during cyclonic storms: Hurricane Ike (2008), Texas Gulf Coast, USA. *Geology*, 38(4), 351–354.
- Hayes, M. O. (1967). Hurricanes as Geological Agents, South Texas Coast: GEOLOGICAL NOTES. *AAPG Bulletin*, 51(6), 937–942.
- Hope, M. E., Westerink, J. J., Kennedy, A. B., Kerr, P. C., Dietrich, J. C., Dawson, C., ... Westerink, L. G. (2013). Hindcast and validation of Hurricane Ike (2008) waves, forerunner, and storm surge. *Journal of Geophysical Research: Oceans*, 118(9), 4424–4460.
- Hosier, P. E., & Cleary, W. J. (1977). Cyclic geomorphic patterns of washover on a barrier Island in southeastern North Carolina. *Environmental Geology*, 2(1), 23–31.
- Houser, C., Hapke, C., & Hamilton, S. (2008). Controls on coastal dune morphology, shoreline erosion and barrier island response to extreme storms. *Geomorphology*, 100, 223–240.
- Johnson, B. D., Kobayashi, N., & Gravens, M. B. (2012). *Cross-Shore numerical model CSHORE for waves, currents, sediment transport and beach profile evolution* (Technical Report No. ERDC/CHL-TR-12-22). Vicksburg, MS: Engineer Research and Development Center.
- Kobayashi, N., de los Santos, F. J., & Kearney, P. G. (2008). Time-averaged probabilistic model for irregular wave runup on permeable slopes. *Journal of Waterway, Port, Coastal, and Ocean Engineering*, 134(2), 88–96.
- Leatherman, S. P., Rampino, M. R., & Sanders, J. E. (1983). Barrier island evolution in response to sea level rise; discussion and reply. *Journal of Sedimentary Research*, 53(3), 1026–1033.
- Lennon, G. (1991). The nature and causes of hurricane-induced ebb scour channels on a developed shoreline. *Journal of Coastal Research*, 237–248.
- Lindemer, C. A., Plant, N. G., Puleo, J. A., Thompson, D. M., & Wamsley, T. V. (2010). Numerical simulation of a low-lying barrier island's morphological response to Hurricane Katrina. *Coastal Engineering*, 57(11-12), 985–995.
- Mason, C. (1981). *Hydraulics and Stability of Five Texas Inlets* (Report No. 81-1) (p. 109). Fort Belvoir, VA: U.S. Army Corps of Engineers Coastal Engineering Research Center.
- McCall, R. T., Van Thiel de Vries, J. S. M., Plant, N. G., Van Dongeren, A. R., Roelvink, J. A., Thompson, D. M., & Reniers, A. J. H. M. (2010). Two-dimensional time dependent hurricane overwash and erosion modeling at Santa Rosa Island. *Coastal Engineering*,

57(7), 668–683.

- Medellin, G., Brinkkemper, J. A., Torres-Freyermuth, A., Appendini, C. M., Mendoza, E. T., & Salles, P. (2015). Runup parameterization and beach vulnerability assessment on a barrier island: a downscaling approach. *Natural Hazards Earth Systems Sciences Discussions*, 3, 3077–3117.
- Morton, R. A., Paine, J. G., & Gibeaut, J. C. (1994). Stages and durations of post-storm beach recovery, southeastern Texas coast, USA. *Journal of Coastal Research*, 884–908.
- Morton, R. A., & Pieper, M. J. (1975). *Shoreline changes in the vicinity of the Brazos river delta (San Luis Pass to Brown Cedar Cut) - An analysis of historical changes of the Texas Gulf shoreline* (No. 75-4) (p. 50). Austin, TX: Texas Bureau of Economic Geology.
- Morton, R. A., & Sallenger Jr., A. H. (2003). Morphological impacts of extreme storms on sandy beaches and barriers. *Journal of Coastal Research*, 19(3), 560–573.
- Paine, J. G., Mathew, S., & Caudle, T. (2012). Historical shoreline change through 2007, Texas Gulf Coast: rates, contributing causes, and Holocene context. *Gulf Coast Association of Geological Societies Journal*, 1, 13–26.
- Roelvink, D., Reniers, A., van Dongeren, A., van Thiel de Vries, J., McCall, R., & Lescinski, J. (2009). Modelling storm impacts on beaches, dunes and barrier islands. *Coastal Engineering*, 56(11-12), 1133–1152.
- Rosati, J. D., & Stone, G. W. (2009). Geomorphologic evolution of barrier islands along the northern U.S. Gulf of Mexico and implications for engineering design in barrier restoration. *Journal of Coastal Research*, 25(1), 8–22.
- Sallenger Jr, A. H. (2000). Storm impact scale for barrier islands. *Journal of Coastal Research*, 16(3), 890–895.
- Sherwood, C. R., Long, J. W., Dickhudt, P. J., Dalyander, P. S., Thompson, D. M., & Plant, N. G. (2014). Inundation of a barrier island (Chandeleur Islands, Louisiana, USA) during a hurricane: Observed water-level gradients and modeled seaward sand transport: Barrier-island inundation. *Journal of Geophysical Research: Earth Surface*, 119(7), 1498–1515.
- Soulsby, R. (1997). *Dynamics of Marine Sands: A Manual for Practical Applications*. Thomas Telford, London.
- Tedesco, L. P., Wanless, H. R., Scusa, L. A., Risi, A. J., & Gelsanliter, S. (1995). Impact of Hurricane Andrew on South Florida's Sandy Coastlines. *Journal of Coastal Research*, (21), 59–82.

- Thieler, E. R., & Bush, D. M. (1991). Hurricanes Gilbert and Hugo send powerful messages for coastal development. *Journal of Geological Education*, 39, 291–298.
- Wang, P., Kirby, J. H., Haber, J. D., Horwitz, M. H., Knorr, P. O., & Krock, J. R. (2006). Morphological and Sedimentological Impacts of Hurricane Ivan and Immediate Poststorm Beach Recovery along the Northwestern Florida Barrier-Island Coasts. *Journal of Coastal Research*, 1382–1402.
- Zhang, K., Douglas, B., & Leatherman, S. (2002). Do Storms Cause Long-Term Beach Erosion along the U.S. East Barrier Coast? *Geology*, 110(4), 493–502.

5.0 Overall project findings

5.1 *Hurricane Ike impact to the dunes and subaerial island*

Hurricane Ike overwashed FI with a 1 m storm surge that lasted 30 hours and a 2.2 m storm surge that lasted over 12 hours. During nearly all of the period of time during the storm surge, there were onshore directed winds and waves. This was followed by a rapid offshore directed storm surge ebb, the initial phase of which was both across the island as well as through the 75 storm surge ebb channels cut through the island. The 12/2008 LIDAR survey shows that the dunes were largely destroyed by Hurricane Ike and that most of the subaerial dunes were flattened.

The modeling study (Chapter 4) found that the bulk of the erosion of FI occurred during the inundation phase of Hurricane Ike and there was significant beach to bay transport of sediment as well as offshore directed sediment transport, both during the inundation phase as well as during the storm surge ebb phase. The impact of the overwash regime had a much greater impact to the eastern end of FI than for the center or western end. This is largely attributed to the dunes on the eastern end being ~0.5 m lower than the rest of the island. This resulted in a significant offshore movement of the shoreline, not seen along the rest of FI.

5.2 *Dune and subaerial Island Recovery*

With the exception of Section C (Fig. 3.4), all sections measured along the FI showed a net gain in sediment volume (up to 25%) after five years of recovery. Each section had a volume recovery of 20-30% from the post-Ike profile. However, on the east end of the island, Sections B & C (Fig. 3.4) experienced an initial volume loss of 20-30% so that they only recovered to approximately the same volume as the pre-Ike profile. Alternatively, in the middle of the island, the sediment volume remained roughly the same immediately after Ike and subsequently increased over the recovery period. The large initial volume loss at Sections B & C is likely caused by the storm surge ebb being more severe at these sections due to their lower elevation. The total subaerial volume of FI increases five years after Hurricane Ike, estimated from LiDAR data, to be 597,153 m³ (Table 4.2). The recovery is largely attributed to across island transport of sand from the bayside to the beach side. As noted above, there was a significant volume of sand that was transported during the storm overwash from the beach side to the bayside. However, there is an average of 47 cold fronts a year that impact this section of the coast and these cold fronts have a very strong northerly wind component. This means that the north shore of FI gets pounded by waves during each of the cold front passages. Although the individual cold fronts are not nearly as strong as a single hurricane, the cumulative effect can be significant. During the 5 year recovery phase there were 200-250 cold fronts, with each front not only eroding the northern bay shoreline of FI, but also blowing sand seaward across the island. We believe this is the primary mechanism for dune and subaerial island recovery. This recovery mode is supported by the observation that the dune volume increased from the

north towards the south during the recovery phase (Fig. 3.5).

5.3 Submarine impact of FI and how this compares to the dune and

The side scan sonar, chirp, swath bathymetry and beach profile data all show an overall trend in that the submarine shoreface of FI experienced net erosion across the island. Furthermore, because the post-storm data was collected five years following the storm, these data reflect not only the impact from the storm but also the recovery period following the storm. We estimate, based off of pre- and post storm beach profiles, that approximately $12 \times 10^6 \text{ m}^3$ of sand was eroded from the shoreface. In some places the shoreface retreated landward up to 180 m. This means that volume of sand accreted within the dunes and across the subaerial portion of the island represents approximately 5% of the total volume of sand lost from the shoreface during Hurricane Ike. Clearly, this 5% is only a portion of the sand that was transported across FI into Christmas Bay. Sediment cores collected from Christmas Bay by Dellapenna's research lab reveal that on the decadal to centennial time scale, revealed by ^{210}Pb geochronology, the sedimentation rates in Christmas Bay are on the order of 1-2 mm/y, suggesting that Christmas Bay is not a significant sink of sand. Taken together, these findings suggest that at least 90% of the volume of sand eroded from the shoreface of FI either moved offshore or along the coast.

6.0 Coring supplement

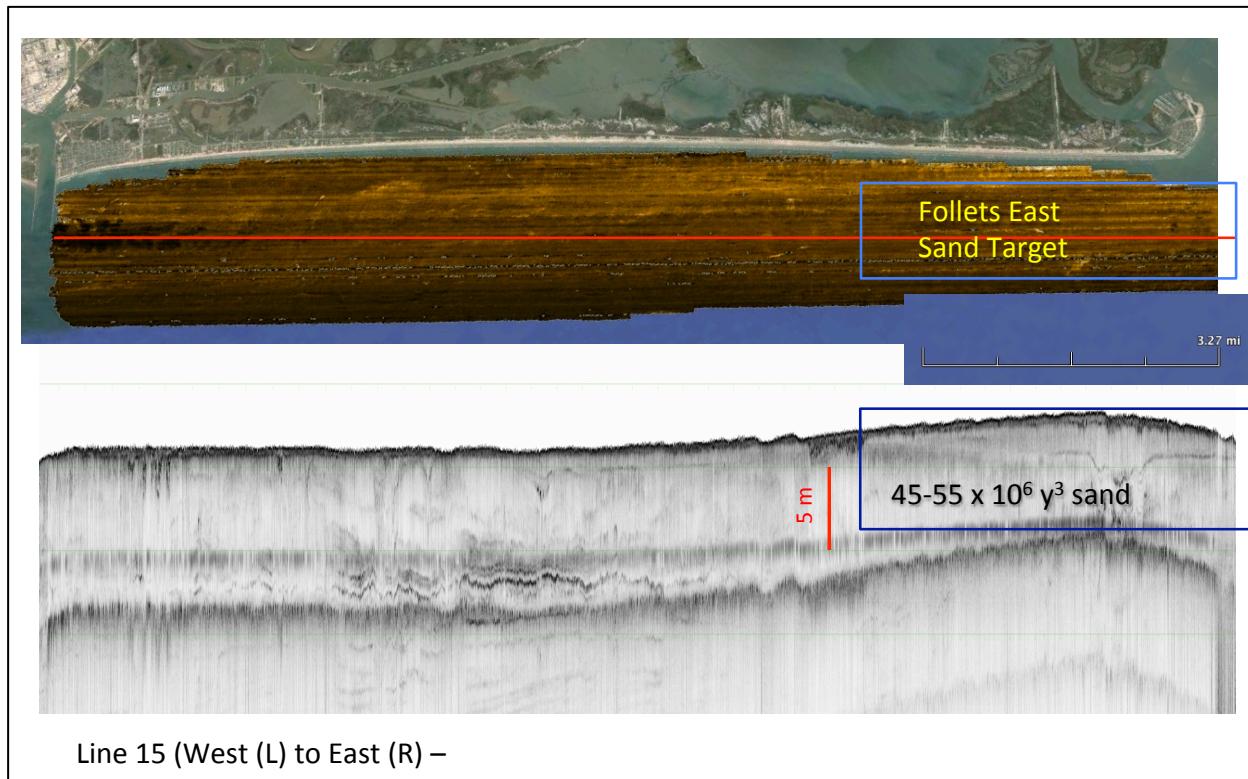


Figure 6.1. Side scan sonar mosaic and CHIRP subbottom profiler line showing the targeted sand deposit for the CMP Cycle 18 Coring Supplement.



Figure 6.2. PVL-Tech vibracoring head

During the course of this study, during the analyses of the CHIRP data, we found what we believe is a significant sand deposit sitting off of the eastern end of the survey area (Fig. 6.1). We received funding from two separate sources to investigate this deposit. We received a CMP Cycle 18 Supplemental Grant to acquire a PVL-Tech submersible vibra corer (Fig. 6.2) that will be used to collect vibro cores from the deposit, and funding to collect 10 cores from this target and also from other sites along FI to ground truth the side scan sonar and CHIRP data. Additionally, we received funding from the Coastal Impact Assistance Program (CIAP) to collect an additional 20 cores. The funding request for the PVL-tech was made in November 2014 with the anticipation that the rig would be purchased in very early 2015 and the cores would be collected and processed during the winter and spring of 2015. However, the contract was held up at NOAA until the end of April 2015. By the time the contract was in place and a purchase order could be placed for the PVL-tech, all of the units from the previous production run had been sold. This delayed

acquisition of the coring unit on June 12. The original plan had been to use the R/V Manta, the NOAA Flower Garden Banks vessel, as a coring vessel, however, it is booked solid in the summer for to support its primary mission.



Figure 6.3. The R/V Trident, TAMUG's new 70 foot long research vessel.

TAMUG took delivery of a new research vessel, the R/V Trident (Fig. 6.3) in June 2015 and it became partially available for research in July 2015. On July 14 we took the R/V Trident out to test the PVL-tech in Galveston Bay. In setting up the coring rig, we damaged a submarine electrical connector and it had to be sent back to the manufacturer for repairs. It was returned from the manufacturer on August 12, and on that day we took it offshore to use for the coring project

(Figs 6.5 & 6.6). With every attempt on collecting a core, the coring rig fell over and bent or damaged the pipe. After a full day of attempting to collect cores, it was decided that we needed a different approach to using the rig and we returned without any cores.



Figure 6.4. The R/V Big Daddy, TAMUG's 30 foot long motorized coring barge.



Figure 6.5. PVLI-Tech hanging from A-Frame aboard the R/V Trident, being tested on July 14.

On August 18 we attempted a second practice cruise in Galveston Bay, near our campus. During these attempts, the rig also fell over rather than penetrating the seabed. It was unclear whether the problem was the inability of the vessel to hold position or if the problem was with the rig. To test this, we took the R/V Big Daddy, a 30 foot coring barge off shore to the study site to attempt to collect cores. The R/V Big Daddy is a much smaller vessel and can easily be placed on a four point anchor mooring, where the position can be held. After several attempts

to collect cores, it was determined that the bottom was too hard to collect cores without a frame that will hold the core barrels upright while the cores are collected.



Figure 6.6. PVL-Tech vibra coring head on work bench while students mount core barrel to it.

The manufacturer does not sell these frames, they have to be custom made. After reviewing frames used by others for this purpose, we designed a frame that will be able to be used on both of the vessels from which we core, the R/V Trident and the R/V Big Daddy.

We ordered materials and supplies for the building of the frame and completed the building of the frame (Figs. 6.7) on Sept. 21.

Unfortunately, weather conditions during the remainder of Sept. were too rough to go offshore to collect the required cores.

Typically, from mid-Sept. to mid-October, the weather transitions from Summer to Fall conditions and tend to be rough. Once the cold front season starts in mid October, there are weather windows right after the cold front where seas are very calm. The cores will be collected in conjunction with the next series of CIAP coring cruises this Fall (2015). Results will be incorporated into a revised report to CMP once completed.



Figure 6.7. The submersible vibra coring frame built by the TAMUG Coastal Geology Laboratory to support submersible vibra coring so that the core head will not fall over.